

Fluctuations and Response in Non-reciprocal Biophysical Models

ICTP Diploma Thesis

Kristian Angeli T. Pajanonot

Postgraduate Diploma
Quantitative Life Sciences
The Abdus Salam International Centre for Theoretical Physics
Trieste, Italy

Supervisors:

Dr. Edgar Roldan

Dr. Sarah Loos

18 August 2022

Abstract

Physical interactions between particles that are coupled are typically reciprocal, i.e. obeys Newton's third law, action = reaction. Such systems can achieve thermal equilibrium in the absence of driving forces or temperature gradients. However, the idea of reciprocal couplings breaks down in many living systems. An illustration of this are birds in a flock, who adjust their flying patterns in reaction to the birds in front of it. So, bird B (back) sees bird A (front) and reacts to its movement, but bird A does not react to B, simply because it cannot see bird B. These non-reciprocal interactions appear as non-conservative forces in the equations of motion and drive the system away from equilibrium. In this work, we take two biophysical models: (1) a hair bundle model where the position and the active force generated by the molecular motors have a bidirectional non-reciprocal coupling, and (2) a cellular sensor model where a receptor senses a fluctuating ligand concentration, but not the other way around. In this case, the sensor is unidirectionally coupled to the signal. We show that these two systems violate the fluctuation-dissipation theorem (FDT), and have a finite energy dissipation, which are characteristics of non-equilibrium systems. We also show that 2-dimensional systems (x_0 and x_1) with bidirectional non-reciprocal coupling can still reach equilibrium as long as $a_{10}T_0 = a_{01}T_1$ (where T_0 and T_1 are temperatures of the heat baths of x_0 and x_1 , respectively, and x_0 is coupled to x_1 by a_{10} and x_1 is coupled to x_0 by a_{01}), whereas a system with unidirectionally coupling cannot reach an equilibrium state. In addition, we vary the degree of reciprocity between two systems. In isothermal and non-isothermal conditions, the plot of the energy dissipated from the violation of FDT $\langle J \rangle$ and the heat rate $\langle \dot{Q}_0 \rangle$ as a function of a_{01} are symmetric to the point at $a_{01} = 0.5(a_{10}\frac{T_0}{T_1})$. For systems with non-reciprocal interaction, we show that $\langle J \rangle$ is in excellent agreement to the heat flow $\langle \dot{Q}_0 \rangle$ of the degree of freedom that we have perturbed.

Contents

Abstract	i
1 Introduction	1
1.1 Goals and overview of this work	4
2 Theoretical Background	5
2.1 Brownian Motion and Langevin Equation	5
2.1.1 Markovian Langevin Equation	5
2.1.2 Overdamped Langevin Equation	6
2.1.3 Wiener Process, Stochastic Calculus	6
2.2 Non-reciprocal Interactions	7
2.3 Stochastic Energetics	9
2.3.1 Stochastic Heat	10
2.3.2 Heat Rate, Entropy Production as a Measure of Non-equilibrium	10
2.4 Autocorrelation function, Response function, Fluctuation-Dissipation Theorem	11
2.4.1 Autocorrelation function	11
2.4.2 Fluctuation-Dissipation Theorem	12
2.4.3 Violation of FDT as a Measure of Non-equilibrium	13
2.5 Biophysical Models	14
2.5.1 Biophysical Model 1: Hair Bundle Oscillations	14
2.5.2 Biophysical Model 2: Cellular Sensor	16
3 Results and Discussion	19
3.1 2-Dimensional Generic Model	19
3.1.1 Steady-state Probability Density Function	19
3.1.2 Stochastic heat	22
3.1.3 Violation of Fluctuation-Dissipation Theorem	23
3.2 Non-reciprocal interactions: Biophysical Models	25
3.2.1 Model 1: Hair bundle oscillations	25
3.2.2 Model 2: Cellular sensor	34
3.3 Non-reciprocal Interactions: Different Degrees of Reciprocity	37
3.3.1 Isothermal conditions, $T_0 = T_1$	38

CONTENTS	iii
3.3.2 Non-isothermal conditions	40
4 Conclusions	42
Bibliography	44
A Numerical simulation of computing the Autocorrelation function	A-1

CHAPTER 1

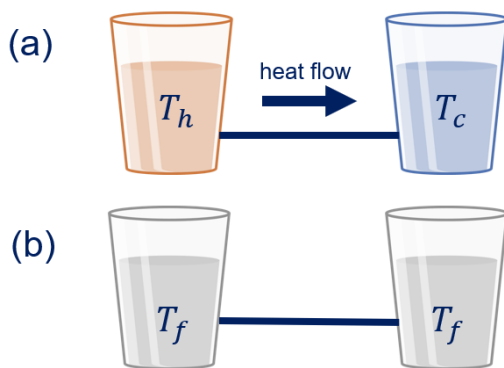
Introduction

In recent years, there has been a lot of interest in extending concepts from statistical physics to understand systems that operate far from equilibrium, including biophysical models (such as: hair bundle - a cell in the ear of bullfrogs [1], flickering of red blood cells [2]) and active matter models (such as self-propelled particles [3]). A far reaching goal is to find a description of these systems from the standpoint of statistical physics and thermodynamics. Here, we consider from this perspective, systems that exhibit non-reciprocal interactions (a type of non-conservative force) found in biophysical models. Since these systems with non-reciprocal interactions are out of equilibrium, we want to understand its properties and to tackle the different methods that we can use to characterize and quantify these non-equilibrium processes.

Equilibrium vs Non-equilibrium system

We begin by reminding our readers of the difference between an equilibrium system and a non-equilibrium system. When one takes two glasses of water at initially different temperatures and put them in thermal contact, one observes a non-equilibrium interaction between these two systems as heat transfer occurs (see Figure 1.1(a)). But after a long time and when no external driving is present, the two glasses of water will eventually reach the same temperature (see Figure 1.1(b)). The two glasses of water reach a thermal equilibrium.

Figure 1.1: (a) Two objects at different temperatures (T_h = hot and T_c = cold) are placed in thermal contact and heat flows from the hot object to the cold object. (b) The final temperature T_f of the two objects are equal after a considerable amount of time(image from [4]).



Another illustration of an equilibrium system could be a system at chemical equilibrium – where the rates of the forward and reverse reactions are equal, and there is no further net change in the concentrations of substrate or product [5].

On the other hand, non-equilibrium systems do not have an equilibrium state. The vast majority of systems in nature are not in thermodynamic equilibrium because they are con-

stantly changing and are subject to the transfer of matter and energy between them and other systems. For example, when you take a look outside your window, you can observe how birds use their wings to move around and search for food, water, and light. In order to live, birds must spend energy (see Figure 1.2). Like all other biological systems, birds are intrinsically out of equilibrium.

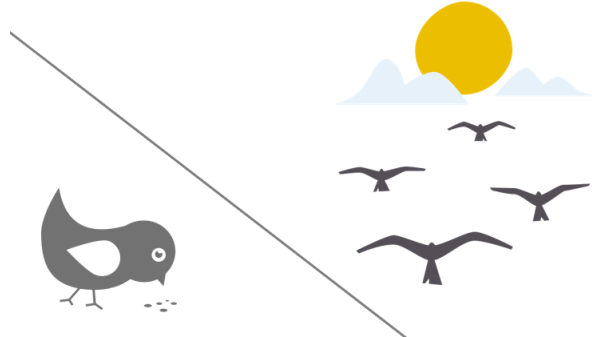


Figure 1.2: Birds must spend energy in order to live - they consume energy when they eat, they dissipate energy when they fly (image from [6]).

We can bring an equilibrium system to a system away from equilibrium by introducing changes in temperature, concentration, or by the application of non-conservative forces. When external non-conservative forces act on a particle, they prevent the system to reach equilibrium, because they continuously pump energy into the system. From the perspective of thermodynamics, ultimately, this energy is dissipated in the form of heat. Thus, a finite net heat flow is a signature of non-equilibrium. Other properties of non-equilibrium systems are also the breaking of time-reversal symmetry, and the violation of the fluctuation-dissipation theorem (FDT) [7, 8]. Based on these, several methods have been established to quantify non-equilibrium processes in biological systems.

Measures of Non-equilibrium

For this work, we consider two measures: the violation of fluctuation-dissipation theorem, and the heat rate. Here, we only give an overview. We will later define the quantities rigorously (see Chapter 2.4 and 2.3).

Violation of the Fluctuation-Dissipation Theorem (FDT) One can compare spontaneous fluctuations to linear response functions, which are related to each other through the FDT. Since FDT is a hallmark for equilibrium systems, when a system is driven out of equilibrium, the FDT is violated. The extent to which a system violates the FDT can provide insight into the non-equilibrium activity in a system. The FDT violation is a sophisticated technique for the detection of activity in biological systems and has been used in studies of: hair bundles in bullfrogs [1], RBC flickering [2], and dissipation in living oocytes [9]. Harada and Sasa then introduced an equality that relates the average energy dissipation with the extent of violation of the FDT in non-equilibrium systems [10].

Heat Rate The "non-equilibriumness" of a system can also be measured from the perspective of energy flows. Two more essential quantitative measurements of a non-equilibrium process are the heat rate and the total entropy production rate. Even if the broken FDT shows that there is non-equilibrium, it does not measure how far away it is. As opposed to this, the total entropy production (EP) directly measures irreversibility, or the breaking of time-reversal symmetry [7]. For non-equilibrium systems, both values are non-zero, while they are both

zero for equilibrium systems.

Non-reciprocal interactions appear as non-conservative forces

Systems that reach thermal equilibrium when no external driving is present implies that interactions between particles are conservative or reciprocal which fulfill Newton's third law, action = reaction. An example of which is a book at rest on the ground (see Figure 1.3(a)). However, reciprocal interactions are often broken in models of many complex living systems [11]. Birds in flocks demonstrate how easy the law can be broken since they alter their flying patterns in reaction to the birds in front of them. As a result, the interactions between the blue bird and the red bird are not reciprocal – the red bird sees the blue bird and responds to the movement of the blue bird, but the blue bird doesn't react to the red bird, simply because it does not see the red bird (see Figure 1.3(b)). Non-reciprocal interactions appear as non-conservative forces in the equations of motion and thus drives the system away from equilibrium [11].

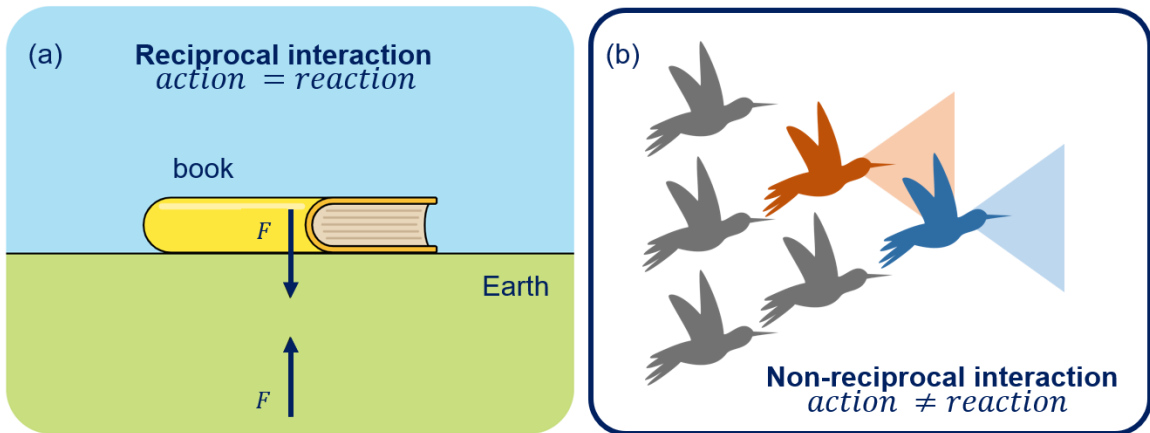


Figure 1.3: (a) There is gravitational force on the book due to Earth and the gravitational force of the book on Earth (action = reaction) (image from [12]). (b) The flock of birds is an example of a system exhibiting non-reciprocal interactions (action \neq reaction). Despite the fact that the red bird sees the blue bird and reacts to its movement, the blue bird does not react to the red bird, simply because it cannot see the red bird (bird icon from [6]).

Among the different types of non-conservative forces, the focus of this work is on non-reciprocal interactions. In addition, we also want to tune the degree of reciprocity between interactions and observe what are the implications. We will study non-reciprocal interactions in small-scale systems which are different from the birds who are macroscopic. We will focus on two biophysical models: a hair bundle (i.e., a cell in the ear), and a cellular sensor model.

Hair bundles found in a frog's auditory canal were the subject of one of the earliest investigations on the violation of FDT in biological systems. Hair bundles (see Figure 1.4(a)) oscillate spontaneously and are assumed to be responsible for the ear's ability to actively filter external inputs and generate sound. In order to do this, hair bundles require an active energy source. The active mechanism that amplifies the sound is carried out by the molecular motors found inside the hair bundle[1, 13, 14]. These oscillations can be described by the interaction between the position of the hair bundle and the active force generated by the molecular motor which are non-reciprocal [8]. The second biophysical model is a cellular sensor model[15] where we have a sensor that measures an external stochastic signal. We

specifically take a set of receptors (sensor) that estimates the concentration of an external ligand (signal) (see Figure 1.4(b)). The interaction between the sensor (receptor) and the measured system, or the signal (external ligand) are non-reciprocal – the sensor depends on the state of the external ligand, but not the other way around.

We will explain the details of the models in Chapter 2.

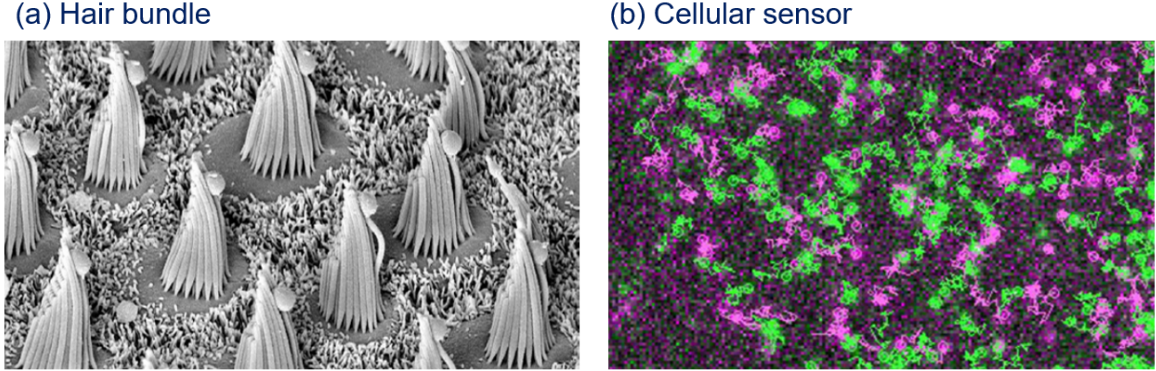


Figure 1.4: (a) **Hair bundle** Image of hair bundles protruding from the apical epithelial surface of the bullfrog’s ear using scanning electron microscopy (image taken from [16]) (b) **Cellular sensor** Image of receptors (green) in the cell membrane of living cells using single-molecule microscopy (image taken from [17]). In this image, the receptor is interacting with G protein (violet). In our model, we consider the receptor sensing an external ligand concentration.

1.1 Goals and overview of this work

The best description we have to date for complex processes on the nano- to micrometer scale is stochastic modeling [7]. Brownian motion, in particular stochastic modeling via the Langevin equation, are not restricted to systems in thermal equilibrium but can also be utilized to simulate other active particles (living or artificial matter).

In this work, we study 2-dimensional systems of overdamped Markovian Langevin equations that exhibit non-reciprocal interactions. We analytically solve for the autocorrelation function and response function from which we determine the violation of the FDT. From the violation of the FDT, we can determine the dissipated energy using the Harada-Sasa equality. In addition, we use the concept of energy flows to compute for the heat rate and total entropy production rate. We perform these calculations for our two biophysical models that are in non-equilibrium, specifically exhibiting non-reciprocal interactions. We take an additional step for our hair bundle model by comparing this to a system in equilibrium, i.e., uncoupled. Finally, we determine the dissipated energy for varying degrees of reciprocity between two systems.

CHAPTER 2

Theoretical Background

2.1 Brownian Motion and Langevin Equation

Brownian motion is the irregular, random movement of a Brownian particle (particles of sizes between 10^{-9}m to 10^{-6}m) immersed in a fluid as a result of the collisions it experiences with the much smaller particles (particles of sizes around 10^{-10}m) of the surrounding fluid. It was Robert Brown in 1827 that first discovered that pollen grains when suspended in water were in a zigzag, irregular motion under a microscope. Einstein in 1905, then developed a theory for an ensemble of Brownian particles moving in one dimension, showing the following important properties [14]:

- average position vanishes at any time $\langle x(t) \rangle = 0$
- average mean square displacement depends linearly on time $\langle x^2(t) \rangle = 2Dt$ (where D is the Diffusion coefficient)

2.1.1 Markovian Langevin Equation

The motion of a Brownian particle in a viscous fluid is mathematically described by the Markovian Langevin equation (see Equation (2.1)). Here, we assume that the Brownian motion has a Markov property, which means that the future evolution of the motion of the Brownian particle depends only on the present state of the system, and does not depend on the past states. Hence, the Markov process is called the process with memory-less property, since knowledge of the past states does not provide useful information [7].

$$m\ddot{x}(t) = -\gamma\dot{x}(t) + V'(x(t)) + f(x(t)) + \sqrt{2k_B T \gamma} \xi \quad (2.1)$$

The notation $\dot{x}(t)$ denotes taking the derivative with respect to time, and will be used throughout this project.

From Equation (2.1), $m\ddot{x}(t)$ is the inertia term where m is the mass of the Brownian particle, and $\ddot{x}(t)$ is its acceleration. The force acting on the Brownian particle is a sum of four terms: the Brownian particle is trapped in a potential $V(x(t))$, with an external force $f(x(t))$ acting on the particle. $-\gamma\dot{x}(t)$ is the Stokes' friction force - the viscous force that the surrounding fluid exerts on the Brownian particle proportional to its velocity, and $\sqrt{2k_B T \gamma} \xi$ is a noise term with $\sqrt{2k_B T \gamma}$ noise strength that represents the fluctuating forces experienced by the Brownian particle from the surrounding fluid. ξ is the Gaussian white noise.

2.1.2 Overdamped Langevin Equation

In the case when the inertia of the Brownian particle is negligible in comparison with the friction force, the trajectory of the Brownian particle is described by the overdamped Langevin equation:

$$\gamma \dot{x}(t) = V'(x(t)) + f(x(t)) + \sqrt{2k_B T \gamma} \xi \quad (2.2)$$

This one-dimensional system can be extended to multidimensional systems by replacing x by a vector $\underline{X} = \{x_0, x_1, \dots, x_n\}$, V by a vector $\underline{V} = \{V_0, V_1, \dots, V_n\}$, f by a vector $\underline{F} = \{f_0, f_1, \dots, f_n\}$ and the noise ξ by a vector $\underline{\xi} = \{\xi_0, \xi_1, \dots, \xi_n\}$. For this project, we will only be dealing with systems in the overdamped limit.

2.1.3 Wiener Process, Stochastic Calculus

Let us consider the overdamped Langevin Equation below:

$$\gamma \dot{x}(t) = F + \sqrt{2k_B T \gamma} \xi \quad (2.3)$$

We can rewrite Equation (2.3) as a stochastic differential equation of the form:

$$\gamma dx(t) = F dt + \sqrt{2k_B T \gamma} dW(t) \quad (2.4)$$

where $W(t)$ is called the Wiener process.

Wiener Process Wiener process is the idealized mathematical representation of Brownian motion. The Wiener process is a stochastic process having the following properties [14]:

- $W(0) = 0$
- $W(t)$ is continuous in time
- $W(t)$ process has independent, Gaussian distributed increments $dW(t) = W(t + \Delta t) - W(t)$
- has zero mean $\langle W(t + \Delta t) - W(t) \rangle = 0$
- has correlation of the form $\langle W(t)W(t + \Delta t) \rangle = D_x \delta(t - t')$ with amplitude D_x

Itô vs. Stratonovich Stochastic calculus decides on the question of how to interpret integrals of the type $\int_0^t g(X(s), s) dW(s)$, for some arbitrary function g . Two common choices are Ito, the starting-point rule, and Stratonovich, the mid-point rule [18, 19, 20].

Calculus of Itô type:

$$\int_0^t g(X(s), s) \cdot dW(s) = \lim_{N \rightarrow \infty} \sum_{i=0}^{N-1} g(X_i, t_i) \Delta W_i \quad (2.5)$$

Calculus of Stratonovich type:

$$\int_0^t g(X(s), s) \circ dW(s) = \lim_{N \rightarrow \infty} \sum_{i=0}^{N-1} g\left(\frac{X_i + X_{i+1}}{2}, \frac{t_i + t_{i+1}}{2}\right) \Delta W_i \quad (2.6)$$

Numerical Integration of Stochastic Differential Equations Not all stochastic differential equations can be solved analytically. Often, we solve these equations with the help of a computer - a process called numerical simulation. Euler Scheme [21] is one method to numerically integrate the stochastic differential equation of the form:

$$dX(t) = f(X, t)dt + g(X, t)dW(t) \quad (2.7)$$

where f and g are generic functions, and $W(t)$ is the Wiener process.

Given $X(t)$, the value of the process at $t + \Delta t$ is obtained as follows:

$$X(t + \Delta t) = X(t) + f(X(t), t)\Delta t + g(X(t), t)\Delta W(t) \quad (2.8)$$

where $\Delta W(t) \sim \mathcal{N}(0, \sqrt{\Delta t})$ has a Gaussian distribution with zero mean and standard deviation $\sqrt{\Delta t}$

An approximation of a sample path of the stochastic process $X(t)$ is achieved upon iterating this process and a random number ΔW generated at each time step Δt . The simulation is then repeated across numerous independent trials up to a time T , producing a histogram of $X(T)$ values that can be used to approximate the probability density for $X(T)$, and to determine the mean and variance.

The Euler Scheme is used all through out this work.

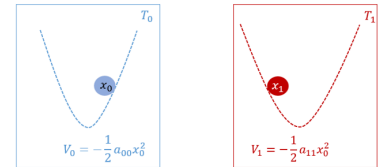
2.2 Non-reciprocal Interactions

Non-reciprocal interactions are also present in small-scale systems which are different from the birds who are macroscopic. These small-scale systems are described by overdamped Langevin equations. In this work, we only consider two degrees of freedom x_0 and x_1 . The simplest case that we have as an example are two Brownian particles, each is trapped in a potential having their own independent heat baths. These two systems are uncoupled (see Figure 2.1).

Figure 2.1: Two Brownian particles, each is trapped in a potential having their own independent heat baths, T_0 and T_1 . These two systems are uncoupled.

Case 1: Two uncoupled systems

$$\begin{aligned} \gamma_0 \dot{x}_0 &= a_{00}x_0 + \sqrt{2k_B T_0} \xi_0 \\ \gamma_1 \dot{x}_1 &= a_{11}x_1 + \sqrt{2k_B T_1} \xi_1 \end{aligned}$$



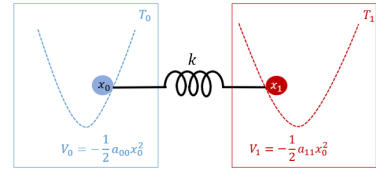
$$a_{00} < 0, a_{11} < 0$$

The second case is when these two systems are coupled by a spring. In this case, the coupling between them is reciprocal (see Figure 2.2).

Case 2: Two systems coupled by a spring (coupling is reciprocal)

$$\begin{aligned}\gamma_0 \dot{x}_0 &= a_{00}x_0 - kx_1 + \sqrt{2k_B T_0} \xi_0 \\ \gamma_1 \dot{x}_1 &= -kx_0 + a_{11}x_1 + \sqrt{2k_B T_1} \xi_1\end{aligned}$$

Figure 2.2: Two Brownian particles, each is trapped in a potential having their own independent heat baths, T_0 and T_1 . These two systems are coupled by a spring.



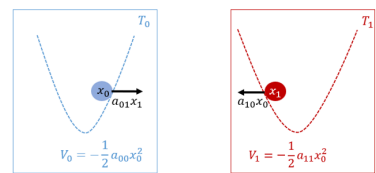
$$a_{00} < 0, a_{11} < 0$$

The third case and the more general case is when the coupling between the two Brownian particles are non-reciprocal — forces $a_{01}x_1$ and $a_{10}x_0$ are acting on particles x_0 and x_1 respectively (see Figure 2.3).

Case 3: Two systems with non-reciprocal coupling

$$\begin{aligned}\gamma_0 \dot{x}_0 &= a_{00}x_0 + a_{01}x_1 + \sqrt{2k_B T_0} \xi_0 \\ \gamma_1 \dot{x}_1 &= a_{10}x_0 + a_{11}x_1 + \sqrt{2k_B T_1} \xi_1\end{aligned}$$

Figure 2.3: Two Brownian particles, each is trapped in a potential having their own independent heat baths, T_0 and T_1 . Force $a_{01}x_1$ is acting on particle x_0 , and force $a_{10}x_0$ is acting on particle x_1 .



$$a_{00} < 0, a_{11} < 0, a_{10} < 0, a_{01} < 0$$

When $a_{10} = a_{01}$, the coupling is reciprocal:

$$\gamma_0 \dot{x}_0 = a_{00}x_0 + a_{01}x_1 + \sqrt{2k_B T_0} \xi_0 \quad (2.9)$$

$$\gamma_1 \dot{x}_1 = a_{10}x_0 + a_{11}x_1 + \sqrt{2k_B T_1} \xi_1 \quad (2.10)$$

Equations (2.9) and (2.10) can be rewritten as derivatives of a potential V + noise (we recall that a potential is a conservative force).

$$\gamma_0 \dot{x}_0 = \frac{-\partial V}{\partial x_0} + \sqrt{2k_B T_0} \xi_0 \quad (2.11)$$

$$\gamma_1 \dot{x}_1 = \frac{-\partial V}{\partial x_1} + \sqrt{2k_B T_1} \xi_1 \quad (2.12)$$

However, for non-reciprocal coupling ($a_{01} \neq a_{10}$), Equation (2.9) and (2.10) cannot be expressed as derivatives of potential V anymore. In this case, $a_{01}x_1$ and $a_{10}x_0$ appear as non-conservative forces in Equation (2.9) and (2.10), respectively. Thus, the dynamics of x_0 and x_1 is not conservative in the presence of nonreciprocal coupling.

Hence, systems with non-reciprocal coupling have the form (where f_{nc} refers to non-conservative force):

$$\gamma_0 \dot{x}_0 = \frac{-\partial V}{\partial x_0} + f_{nc} + \sqrt{2k_B T_0} \xi_0 \quad (2.13)$$

$$\gamma_1 \dot{x}_1 = \frac{-\partial V}{\partial x_1} + f_{nc} + \sqrt{2k_B T_1} \xi_1 \quad (2.14)$$

These non-reciprocal interactions appear as non-conservative forces in our equations of motion.

We also recall that the work done by a conservative force on a “closed path” is zero. And is non-zero for a non conservative force.

Conservative forces

$$\oint F \circ dx = \int -\partial_x V \circ dx = 0 \quad (2.15)$$

Non-conservative forces

$$\oint F \circ dx = \underbrace{\int -\partial_x V \circ dx}_{=0} + \int f_{nc} \circ dx \neq 0 \quad (2.16)$$

We have already mentioned in the Introduction that when external non-conservative forces act on the particle, they prevent the system to reach equilibrium, because they continuously pump energy into the system. From the perspective of thermodynamics, ultimately, this energy is dissipated in the form of heat. Thus, a finite energy dissipation or heat flow is a signature of non-equilibrium.

Can thermal equilibrium exist when there are non-reciprocal interactions? Our initial guess is no, since non-reciprocal interactions appear as non-conservative forces in the equations of motion. However, Loos, et.al [11] showed that there is a special case, where a temperature gradient is introduced in the system. In this case,

$$a_{10}T_0 = a_{01}T_1 \quad (2.17)$$

this condition shows that the temperature gradient and the non-reciprocity can somehow cancel each other and the system reaches an equilibrium state, i.e., FDT can still hold, and there is no energy dissipation.

Thus, non-reciprocal couplings can reach thermal equilibrium following the condition shown in Equation (2.17), as long as $a_{10}a_{01} > 0$. However, systems with unidirectional coupling, such as in the case for a cellular sensor model (where $a_{10} = 0$) does not reach thermal equilibrium, and are non-equilibrium models. Thus, Equation (2.17) implies that non-reciprocal systems can reach equilibrium even when T_0 is different from T_1 .

We now proceed with the discussion of the two measures of non-equilibrium: stochastic heat and violation of FDT.

2.3 Stochastic Energetics

Ken Sekimoto extended the notions of heat and work that we learned in thermodynamics to systems described by Langevin equation [20]. A system, a thermal environment, and an external agent comprises the fluctuating world described by a Langevin equation. These three elements exchange energy along a single realization of a stochastic process. Heat is the energy exchanged between the system and the thermal environment.

2.3.1 Stochastic Heat

We consider again the overdamped Markovian Langevin equation given in Equation (2.1), where the sum of all forces acting on the particle is 0:

$$0 = -\gamma \dot{x}_t + \underbrace{V'(x(t)) + f(x(t))}_{\text{total force, } F(x(t))} + \sqrt{2k_B T \gamma} \xi \quad (2.18)$$

The forces exerted by the thermal environment on the particle, are the friction force $-\gamma \dot{x}$ and the fluctuations $\sqrt{2k_B T \gamma} \xi$. Therefore, the energy transfer from the environment to the particle is:

$$\delta Q = (-\gamma \dot{x} + \sqrt{2k_B T \gamma} \xi) \circ dx \quad (2.19)$$

which we refer to as the heat transferred to the particle in the small interval $[t, t + dt]$ when it is displaced dx . We use the Stratonovich product. We assign a positive sign for an energy flowing from the thermal environment to the particle.

However, ξ cannot be measured experimentally in the laboratory. Instead we write the stochastic heat as

$$\begin{aligned} \delta Q &= -F(x(t)) \circ dx \\ \delta Q &= -(V'(x(t)) + f(x(t))) \circ dx \end{aligned} \quad (2.20)$$

which we can compute or can be measured in the laboratory.

Since our systems of equations is given as:

$$\begin{aligned} \gamma_0 \dot{x}_0 &= a_{00}x_0 + a_{01}x_1 + \sqrt{2k_B T_0} \xi_0 \\ \gamma_1 \dot{x}_1 &= a_{10}x_0 + a_{11}x_1 + \sqrt{2k_B T_1} \xi_1 \end{aligned}$$

Then the stochastic heat for particle x_0 is shown as:

$$\delta Q_0 = -(a_{00}x_0 + a_{01}x_1) \circ dx_0 \quad (2.21)$$

Similarly, the stochastic heat for particle x_1 is:

$$\delta Q_1 = -(a_{10}x_0 + a_{11}x_1) \circ dx_1 \quad (2.22)$$

2.3.2 Heat Rate, Entropy Production as a Measure of Non-equilibrium

Heat Rate

Numerical simulation We calculate the heat rate as given by

$$\langle \dot{Q} \rangle = \lim_{t \rightarrow \infty} \frac{\langle Q(t) \rangle}{t} \quad (2.23)$$

In numerical simulations, heat rate is calculated by taking the slope of its average cumulative stochastic heat (i.e., we compute the value of the cumulative stochastic heat of a long trajectory averaged over many realizations $\langle Q \rangle$ and we divide by time). We use the stochastic heat from Sekimoto's framework [20].

Analytical solution As shown in Ref.[11], the analytical solution for the heat rate of particle x_0 is given as:

$$\langle \dot{Q}_0 \rangle = k_B \frac{a_{01}(a_{10}T_0 - a_{01}T_1)}{a_{00}\gamma_1 + a_{11}\gamma_0} \quad (2.24)$$

The analytical solution of the heat rate for x_1 is symmetric with $\langle \dot{Q}_0 \rangle$, and is given as:

$$\langle \dot{Q}_1 \rangle = k_B \frac{a_{10}(a_{01}T_1 - a_{10}T_0)}{a_{00}\gamma_1 + a_{11}\gamma_0} \quad (2.25)$$

This convention is opposite to the convention used in the numerical simulation, where a positive sign means the energy is flowing from the particle to the heat bath.

Total entropy production rate

Numerical simulation The total entropy production rate [11] (total EPR) is given as:

$$\text{total EPR} = \frac{-\langle \dot{Q}_0 \rangle}{T_0} + \frac{-\langle \dot{Q}_1 \rangle}{T_1} \quad (2.26)$$

where $\langle \dot{Q}_0 \rangle$ and $\langle \dot{Q}_1 \rangle$ refers to the heat rate of particle x_0 and particle x_1 , respectively. We take the negative sign since entropy production is positive.

2.4 Autocorrelation function, Response function, Fluctuation-Dissipation Theorem

2.4.1 Autocorrelation function

The autocorrelation function is an important quantity that we can use to characterize the fluctuations of a Brownian particle. Suppose we want to measure the position of the Brownian particle, x for many samples in the equilibrium state. Let $x(t)$ be the position of the particle at time t . Figure 2.4(a) shows a sample trajectory of the particle. We define the position autocorrelation function, for a process with zero mean, as the average of the product over many measurements [22].

$$C_x(t) = \langle x(t)x(t + \tau) \rangle \quad (2.27)$$

At $t=0$, $C(0)$ is positive and is equal to $\langle x(t)^2 \rangle$. $C(t)$ usually decreases as time passes since the value of $x(t + \tau)$ becomes uncorrelated to that at time $= t$. After a sufficiently long time, the correlation between $x(t)$ and $x(t + \tau)$ vanishes and equals $\langle x(t) \rangle \langle x(t + \tau) \rangle = \langle x(t) \rangle^2$, which is zero for Brownian motion.

Figure 2.4(b) shows a typical behavior of a normalized $C(t)$, given by $C(t)/\langle x(t)^2 \rangle$. At $t = 0$, $C(0)$ is 1. After a sufficiently long time, the correlation approaches to 0.

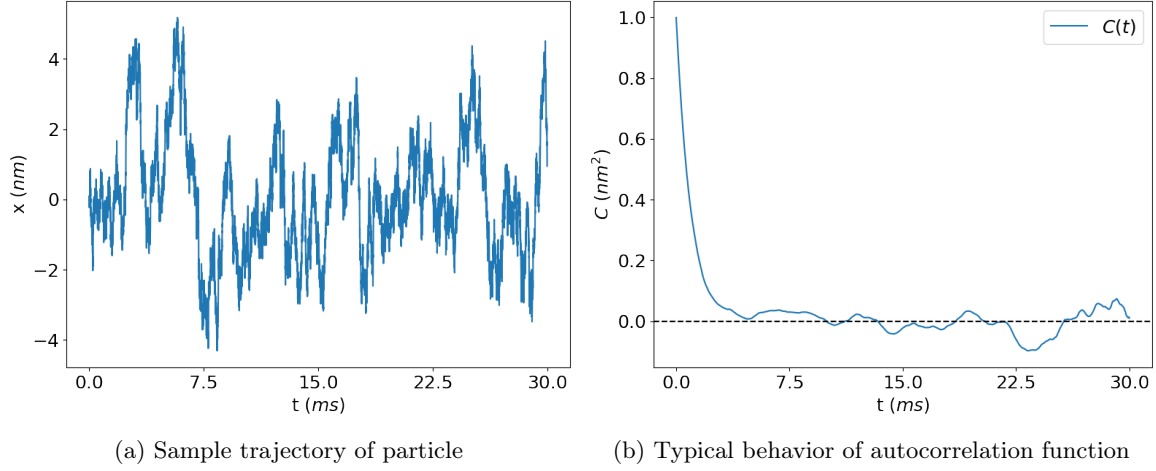


Figure 2.4: (a) Trajectory of an overdamped Brownian particle following an Ornstein-Uhlenbeck process ($\dot{x} = -kx + \sqrt{2k_B T \gamma} \xi$, i.e., the Brownian particle is in a harmonic trap with stiffness k). (b) Corresponding normalized position autocorrelation $\langle x(t)x(t+\tau) \rangle$ with values of τ from 1 up until the length of the trajectory with step size of 30, averaged over 100 realizations. The parameters used to simulate (a) are $k = 1$, $T = 300K$, $k_B = 1.38 \cdot 10^{-2}$ pN nm, $\gamma = 1$. Simulation time step is $\Delta t = 0.001\text{ms}$ with observation time = 30ms, and 100 realizations.

This is called autocorrelation function since it demonstrates the correlation of the same physical quantity at different times. When instead we take the physical quantity velocity v , then $\langle v(t)v(t+\tau) \rangle$ is the velocity autocorrelation function.

2.4.2 Fluctuation-Dissipation Theorem

Consider a system in equilibrium being subjected to a time-dependent external force $F(t)$. $F(t)$ perturbs the system and changes the average values of physical quantities from those in equilibrium state. If the force applied is weak, the change in any physical quantity is a linear functional of the force, and is written as [23]:

$$\langle x(t) \rangle = \int_0^t R_x(t-t')F(t')dt' \quad (2.28)$$

where $\langle x(t) \rangle$ denotes the value of x at time t when the force is applied. The function $R(t)$ is called the response function.

For a system at thermal equilibrium, the Fluctuation-Dissipation Theorem (FDT) relates the autocorrelation function ($C(t)$) to the response function ($R(t)$):

$$R(t) = -\frac{1}{k_B T} \frac{dC(t)}{dt} \quad (2.29)$$

Taking the Fourier transform of Equation (2.29), we can rewrite this as [1]:

$$\tilde{C}_x(\omega) = \frac{2k_B T}{\omega} \tilde{R}_x''(\omega) \quad (2.30)$$

where $\tilde{R}''(\omega)$ is the imaginary or dissipative part of the response function, k_B is the Boltzmann constant, and T is the temperature.

One can examine the micromechanical characteristics of viscoelastic materials, such as biological cells, biopolymers, and gels by observing the motion of minute probe particles (of size micro- to nanometer) embedded in the sample. We can either track the motion of probe particles due to spontaneous fluctuations $C(t)$, or measure the response $R(t)$ of probe particles to an oscillating optical trapping force [24]. Because the experimental duration is brief in some cases, it can be challenging to measure $C(t)$.

2.4.3 Violation of FDT as a Measure of Non-equilibrium

Equilibrium systems obey the FDT. However, FDT is broken for non-equilibrium systems. Consequently, the degree to which a system deviates from the FDT might shed light on its non-equilibrium behavior.

Effective Temperature

As a measure of the degree of violation of the FDT, Martin, et al [1] introduced the frequency-dependent "effective temperature", which is the ratio of fluctuations to dissipation:

$$\frac{T_{EFF}(\omega)}{T} = \frac{\omega \tilde{C}_x(\omega)}{2k_B T \tilde{R}_x''(\omega)} \quad (2.31)$$

T_{EFF} is the temperature at which the FDT holds at angular frequency ω , and it can either be positive or negative. $T_{EFF} = T$ for a system in thermal equilibrium. However, for a system at non-equilibrium, such as the actively driven hair bundle, then T_{EFF} deviates from T at some frequencies.

Energy Dissipation Rate from the Violation of FDT

Harada and Sasa found that for a class of Langevin equations, the rate of energy dissipation from the system to the bath is related to the extent of violation of FDT in the non-equilibrium steady state [10] by:

$$\langle J \rangle = \gamma \int_{-\infty}^{+\infty} \frac{d\omega}{2\pi} \left(\tilde{C}_v(\omega) - 2k_B T \tilde{R}'_v(\omega) \right) \quad (2.32)$$

where $\langle J \rangle$ is the average rate of energy dissipation, γ is the friction coefficient, $\tilde{C}_v(\omega)$ is the Fourier transform of the velocity autocorrelation function, and $\tilde{R}'_v(\omega)$ is the real part of the Fourier transform of the response function.

The velocity is not an observable quantity that can be directly measured in experiments, in contrast to the position. Thus, we rewrite Equation (2.32) to position measurements [8]:

$$\langle J \rangle = \gamma \int_{-\infty}^{+\infty} \frac{d\omega}{2\pi} \left(\omega^2 \tilde{C}_x(\omega) - 2k_B T \omega \tilde{R}_x''(\omega) \right) \quad (2.33)$$

where $\tilde{C}_x(\omega)$ is the Fourier transform of the position autocorrelation function, and $\tilde{R}_x''(\omega)$ is the imaginary part of the Fourier transform of the response function. The Fourier-transformation is defined as: $\tilde{A}(\omega) = \int_{-\infty}^{+\infty} dt a(t) e^{i\omega t}$.

The right hand side of Equation (2.33) vanishes at equilibrium systems because of FDT. However, in general, this is non-zero for non-equilibrium systems.

Now, Equation (2.33) contains quantities that can be accessed experimentally such as the autocorrelation function and the response function, which allows us for a direct estimation of the rate of energy dissipation.

Relation between Heat Rate and Energy Dissipation Rate from the Violation of FDT

In the case of 1-dimensional Langevin equation, $\langle J \rangle = \langle \dot{Q} \rangle$. How does this relation change when we have a non-reciprocal system exhibiting non-reciprocal interactions? Does $\langle J \rangle = \langle \dot{Q}_0 \rangle$? Does it give us the heat flow for the degree of freedom that we perturb?

2.5 Biophysical Models

We now take the two biophysical models introduced in Chapter 1 and discuss in details:

2.5.1 Biophysical Model 1: Hair Bundle Oscillations

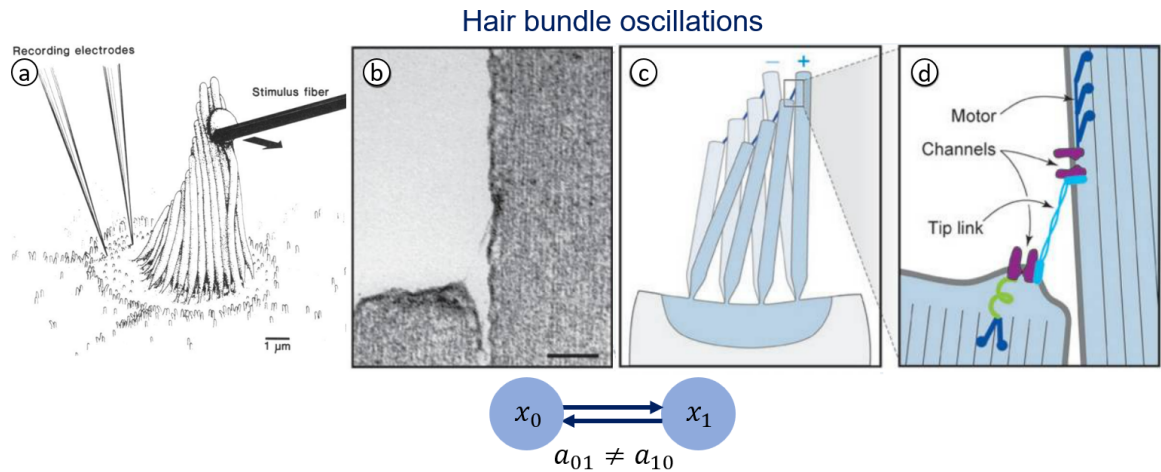


Figure 2.5: **Hair bundle oscillations model** (a) Diagram of a hair bundle in a bullfrog saccule which comprises around 60 stereocilia, with two electrodes positioned at the base to measure the electric current resulting from the displacement of the bundle. (image taken from [13]) (b) Magnified image of two stereocilia with the tip link connecting them (scale bar = $0.1 \mu\text{m}$). (c) When a sound enters the ear, the stereocilia bend at their base and the hair bundle is deflected. (d) Due to the increased tip link tension caused by the deflection, a transduction channel is pulled open at each end. To restore the resting tension, myosin motors slip or climb - a process called adaptation. The dynamics of the hair bundle oscillations can be described by the interaction between the position of the hair bundle (x_0) and the active force generated by the molecular motor (x_1) that have a bidirectional non-reciprocal coupling, $a_{01} \neq a_{10}$ [8] (image taken from [25]).

The hair bundles (a type of cell in the ear) in the bullfrog's sacculus have the ability to oscillate spontaneously. To answer the question whether the spontaneous motion of these hair bundles are active or passive processes, Martin, et.al, [1] studied the oscillations of hair bundles experimentally by tracking the dynamics of hair bundle. In order to do this, a flexible glass fiber was attached to the tip of the bundle to measure the position autocorrelation function and the corresponding reaction to periodic external stimuli (see Figure 2.5). Surprisingly, the magnitude of position fluctuations was found to be far more than the linear-response based

levels, for a purely thermal system. This FDT violation indicates that there is an internal energy source keeping the system away from equilibrium.

From this experimental work, Berger, et. al [8] introduced a model that can adequately describe the hair bundle oscillations. x corresponds to the position of hair bundle (x_0), and F corresponds to the force generated by the active process in the hair bundle (x_1).

Before we proceed to the model, we briefly discuss the physical origin of this active process: Hair bundles are formed by an ensemble of stereocilia connected by tip links. When a sound enters the ear, the stereocilia bend at their base and the hair bundle is deflected. Due to the increased tip link tension caused by the deflection, a transduction channel is pulled open at each end. To restore the resting tension, myosin motors slip or climb - a process called adaptation. With this, the obvious candidate for the force-generating component in the hair bundle is the molecular motors present inside the stereocilia. These motors are also responsible for the active mechanism that amplifies the sound [1, 13, 14, 25].

The model introduced in Ref.[8] is a two-dimensional system of Langevin equations is as follows:

The position x of a hair bundle is given as:

$$\gamma \dot{x} = -kx + F + \eta_x \quad (2.34)$$

where γ is an effective drag coefficient, k a stiffness, and F an active driving force that is generated in the bundle. The noise term η_x describes the fluctuations of the thermal environment that the bundle experiences.

A molecular machinery generates the active force F inside the bundle. This evolves in time according to:

$$\lambda \dot{F} = -\bar{k}x - F + \eta_F \quad (2.35)$$

where λ is the relaxation time, \bar{k} is the coupling constant, and the noise term η_F that stems from the molecular motors having non-equilibrium fluctuations.

The position of the hair bundle x_0 and the active force generated by the molecular motor x_1 are non-reciprocally coupled.

We show in Figure 2.6 sample trajectories of x , F . We also plot x vs F . The sample trajectories of x and F has a characteristic oscillatory behavior.

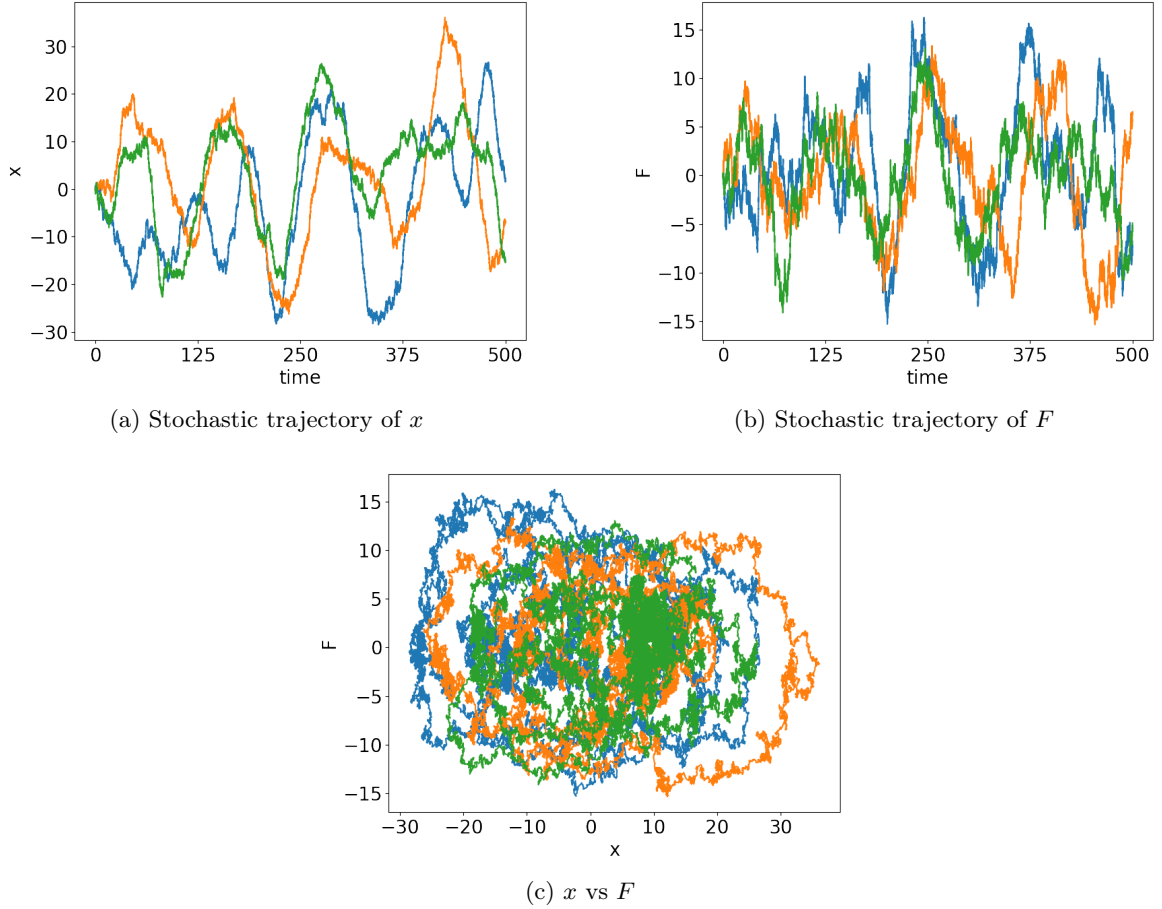
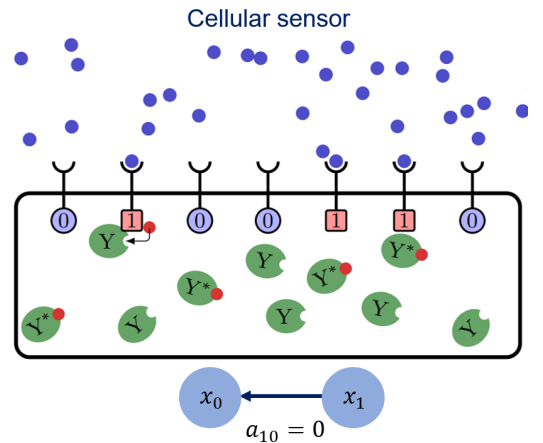


Figure 2.6: Three sample stochastic trajectories of (a) x , (b) y , and (c) x vs F for observation time $t = 500\text{ms}$, with simulation time step $\Delta_t = 0.01\text{ms}$, following the parameters presented in Table 3.1

2.5.2 Biophysical Model 2: Cellular Sensor

Figure 2.7: **Cellular sensor model** [15] with the receptors as the sensor (x_0), and the external ligand concentration as the signal (x_1). The interaction between x_0 and x_1 is unidirectionally coupled, with the receptor sensing the ligand, but not the other way around, hence $a_{10} = 0$. For this work, we ignore the memory component of the sensor (Y) (image taken from [15]).



Hartich, et.al, [15] described a cellular sensor model where a sensor learns about an external stochastic signal. The dynamics of the signal x is not affected by the sensor, whereas the dynamics of the sensor r is affected by the signal. They considered the receptor sensing a fluctuating ligand concentration as a physical realization of a sensor.

The signal x is related to the external ligand concentration, and is given as:

$$\dot{x} = -\omega_x x + \xi_x \quad (2.36)$$

where ω_x indicates the rate of ligand concentration

The sensor r which is related to the number of bound receptors is given as:

$$\dot{r} = -\omega_r r + \omega_r x + \xi_r \quad (2.37)$$

where ω_r indicates the rate of binding to a ligand

In Figure 2.7, the total number of receptors is $N_b = 7$ and the number of occupied receptors is $n_b = 3$. In their paper, they have also discussed a cellular sensor model with memory indicated by the number of internal proteins, $N_y = 10$ with $n_y = 4$ of them phosphorylated. But for this work, we will only be considering the sensor without memory hence our model is described by one degree of freedom, i.e., the number of receptors r .

The interaction between r and x is unidirectionally coupled, with the receptor (x_0) sensing the ligand (x_1), but not the other way around, hence $a_{10} = 0$.

Equation (2.36) is an integral differential equation with the solution:

$$x(t) = x_0 e^{-\omega_x t} + e^{-\omega_x t} \int_0^t e^{\omega_x s} \xi_s ds \quad (2.38)$$

When we plug in the value x to the Equation (2.37), we get the following:

$$\dot{r} = -\omega_r r + \omega_r x_0 e^{-\omega_x t} + e^{-\omega_x t} \int_0^t e^{\omega_x s} \xi_s ds + \xi_r \quad (2.39)$$

This is an equation with memory, i.e., the derivative of r at time t depends not only on quantities at time t but also on the past values in the integral term.

We present in Figure 2.8 the trajectories of r , x . We also plot r vs x . In contrast to the trajectories of the hair bundle model, the sample trajectories of r and x does not have clear oscillations. However, we observe a distinct pattern for r vs x .

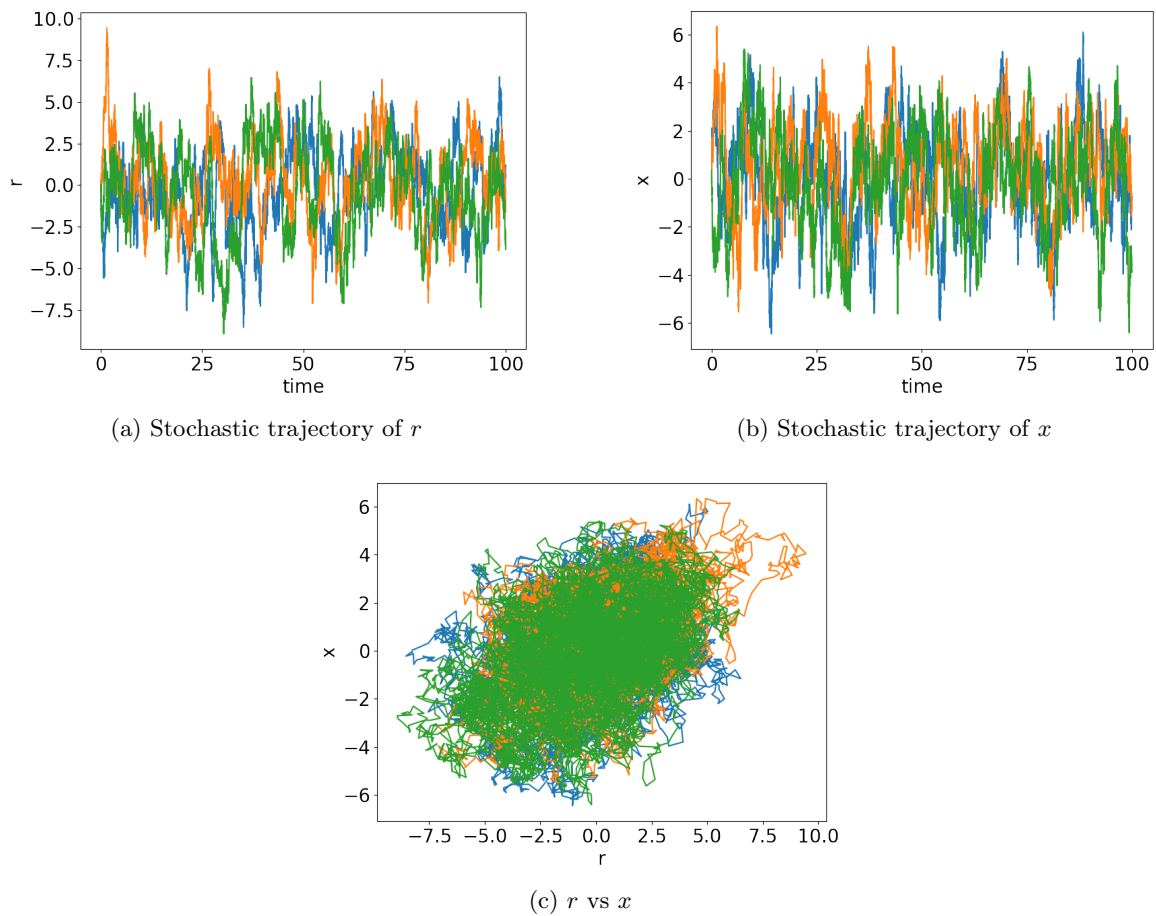


Figure 2.8: Three sample stochastic trajectories of (a) r , (b) x , and (c) r vs x for observation time $t = 100\text{ms}$, with simulation time step $\Delta_t = 0.01\text{ms}$, following the parameters presented in Table 3.5

CHAPTER 3

Results and Discussion

3.1 2-Dimensional Generic Model

For this work, we consider a two-dimensional system described by an overdamped Markovian Langevin equation:

$$\underbrace{\begin{bmatrix} \gamma_0 & 0 \\ 0 & \gamma_1 \end{bmatrix}}_{\underline{\gamma}} \underbrace{\begin{bmatrix} \dot{x}_0 \\ \dot{x}_1 \end{bmatrix}}_{\dot{\underline{x}}} = \underbrace{\begin{bmatrix} a_{00} & a_{01} \\ a_{10} & a_{11} \end{bmatrix}}_{\underline{\underline{A}}} \underbrace{\begin{bmatrix} x_0 \\ x_1 \end{bmatrix}}_{\underline{x}} + \underbrace{\begin{bmatrix} \sqrt{2k_B T_0 \gamma_0} \xi_0 \\ \sqrt{2k_B T_1 \gamma_1} \xi_1 \end{bmatrix}}_{\underline{\xi}} \quad (3.1)$$

Each particle is immersed in a bath at constant temperatures, T_0 and T_1 . ξ_1 and ξ_2 denote zero-mean, Gaussian white noises, with autocorrelation function $\langle \xi_i(t) \xi_j(t') \rangle = 2k_B T_j \gamma_j \delta_{ij} \delta(t - t')$. In addition, the two noise terms are uncorrelated with each other $\langle \xi_i \xi_j \rangle = 0$. k_B is the Boltzmann constant and γ_j is the friction coefficient. The strength of the couplings a_{ij} is defined in the coupling matrix $\underline{\underline{A}}$, and the relaxation time is given as γ_j/a_{jj} . Further, we will focus on cases where the real parts of the eigenvalues of the matrix $\underline{\underline{A}}$ are negative to ensure stability.

We recall that when $a_{01} = a_{10}$ the coupling is reciprocal. When $a_{01} \neq a_{10}$, and $a_{10}T_0 = a_{01}T_1$, the coupling is non-reciprocal but the system is at equilibrium. If $a_{10}T_0 \neq a_{01}T_1$, the system is at non-equilibrium [11].

3.1.1 Steady-state Probability Density Function

We start our comparison between equilibrium and non-equilibrium systems by their steady-state probability density functions (pdfs). Since our model is linear, the steady-state pdfs are multivariate Gaussian distributions [7] defined by the set of parameters: mean vector $\underline{\mu} = 0$, and the covariance matrix $\underline{\underline{\Sigma}}$, which measures how the two variables x_0 and x_1 vary together.

The multivariate Gaussian with dimensionality 2 has a joint pdf given by [11]:

$$f(\underline{x}, \underline{\underline{\Sigma}}) = \frac{1}{\sqrt{|\underline{\underline{\Sigma}}|(2\pi)^2}} \exp \left(-\frac{1}{2} \begin{bmatrix} x_0 \\ x_1 \end{bmatrix}^T \underline{\underline{\Sigma}}^{-1} \begin{bmatrix} x_0 \\ x_1 \end{bmatrix} \right) \quad (3.2)$$

where \underline{x} is a vector of size 2, $\underline{\underline{\Sigma}}$ is the covariance matrix of size 2x2 given in Equation (3.3) and $|\underline{\underline{\Sigma}}|$ is its determinant. The joint pdf shows the probability distribution for x_0 , and x_1 ,

and tells us the relationship between them.

$$\begin{aligned}\underline{\Sigma} &= \begin{bmatrix} \langle x_0^2 \rangle & \langle x_0 x_1 \rangle \\ \langle x_1 x_0 \rangle & \langle x_1^2 \rangle \end{bmatrix} \\ \underline{\Sigma} &= k_B \begin{bmatrix} \frac{T_1 a_{01}^2 - T_0 a_{01} a_{10} + T_0 a_{11} (a_{00} + a_{11} \gamma_0 / \gamma_1)}{(a_{00} + a_{11} \gamma_0 / \gamma_1)(a_{01} a_{10} - a_{00} a_{11})} & \frac{-T_1 a_{00}^2 a_{01}^2 - T_0 a_{11} a_{10} \gamma_0 / \gamma_1}{(a_{00} + a_{11} \gamma_0 / \gamma_1)(a_{01} a_{10} - a_{00} a_{11})} \\ \frac{-T_1 a_{00}^2 a_{01}^2 - T_0 a_{11} a_{10} \gamma_0 / \gamma_1}{(a_{00} + a_{11} \gamma_0 / \gamma_1)(a_{01} a_{10} - a_{00} a_{11})} & \frac{T_0 a_{10}^2 \gamma_0 / \gamma_1 + T_1 a_{00} (a_{00} + a_{11} \gamma_0 / \gamma_1)}{(a_{00} + a_{11} \gamma_0 / \gamma_1)(a_{01} a_{10} - a_{00} a_{11})} \end{bmatrix} \quad (3.3)\end{aligned}$$

When $a_{01} = a_{10}$, Figure 3.1 shows an equilibrium system by having $T_0 = T_1$, and therefore $a_{10}T_0 = a_{01}T_1$. On the other hand, Figure 3.2 shows a non-equilibrium system by having $T_0 \neq T_1$, and therefore $a_{10}T_0 \neq a_{01}T_1$.

We observe that the joint pdf for the non-equilibrium system is more negatively correlated than for the equilibrium system.

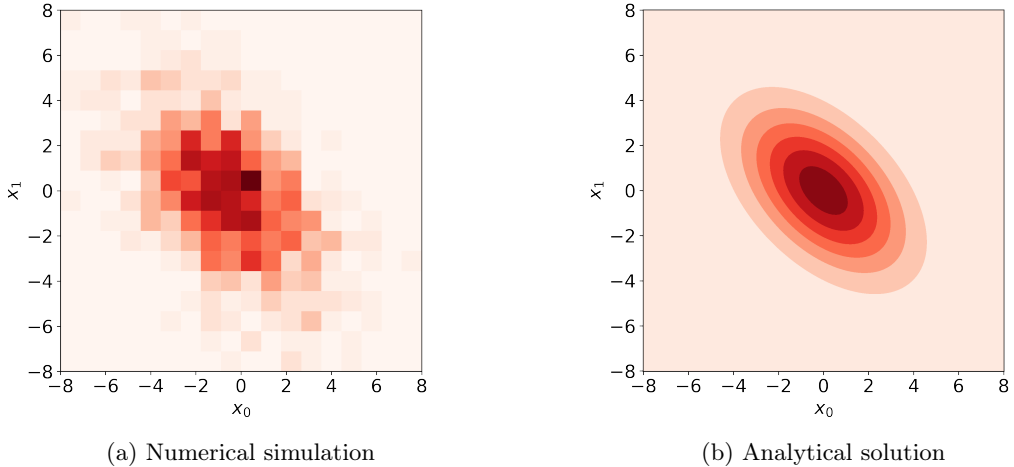


Figure 3.1: **Equilibrium system:** A contour plot of a Gaussian joint probability density function of x_0 and x_1 with (a) Numerical simulation using Euler's numerical simulation scheme, and (b) Analytical solution following Equation(3.2). The darker shaded contour rings in the contour plot indicate higher probability. The parameters used are $a_{00} = a_{11} = -1$, $a_{01} = a_{10} = -0.5$, $T_0 = T_1 = 300K$, $k_B = 1.38 \cdot 10^{-2}$ pN nm, $\gamma_0 = \gamma_1 = 1$. Simulation time step for (a) is $\Delta t = 0.01\text{ms}$ with observation time = 500ms, and 1000 realizations.

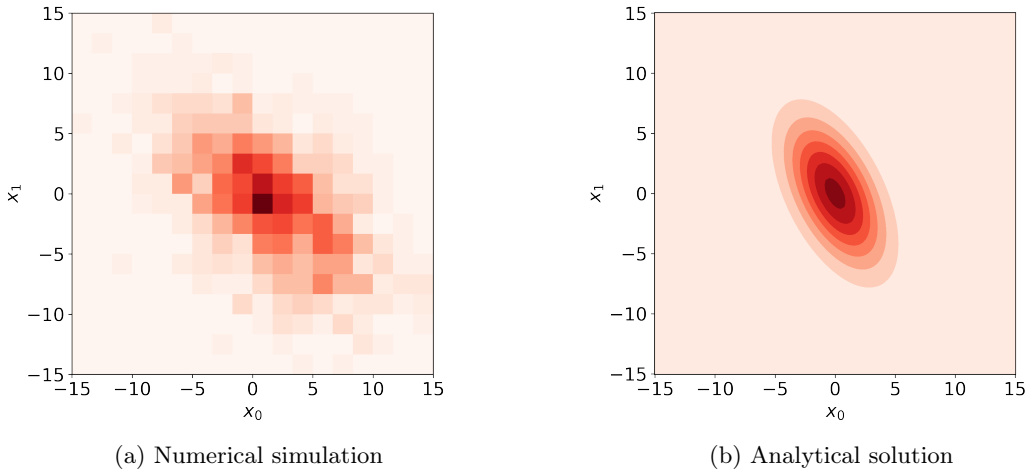


Figure 3.2: Non-equilibrium system: A contour plot of a Gaussian joint probability density function of x_1 and x_2 with (a) Numerical simulation using Euler's numerical simulation scheme, and (b) Analytical solution following Equation(3.2). The darker shaded contour rings in the contour plot indicate higher probability. The parameters used are $a_{00} = a_{11} = -1$, $a_{01} = a_{10} = -0.5$, $T_0 = 300K$, $T_1 = 900K$, $k_B = 1.38 \cdot 10^{-2}$ pN nm, $\gamma_0 = \gamma_1 = 1$. Simulation time step for (a) is $\Delta t = 0.01\text{ms}$ with observation time = 500ms, and 1000 realizations.

A way to check whether the results of the numerical simulation and analytical solution is in agreement is to plot $p_{\text{simulation}}$ (the probability that we obtain from the numerical simulation) vs $p_{\text{theoretical}}$ (the probability that we obtain from the analytical solution). We overlay, a line $y = x$, with slope = 1 on the same plot. When the numerical simulation results and analytical solution results is in agreement, the points $p_{\text{simulation}}$ vs $p_{\text{theoretical}}$ should lie close to the line of slope one.

Figure 3.3 shows that the numerical simulation and analytical solution are in close agreement with each other.

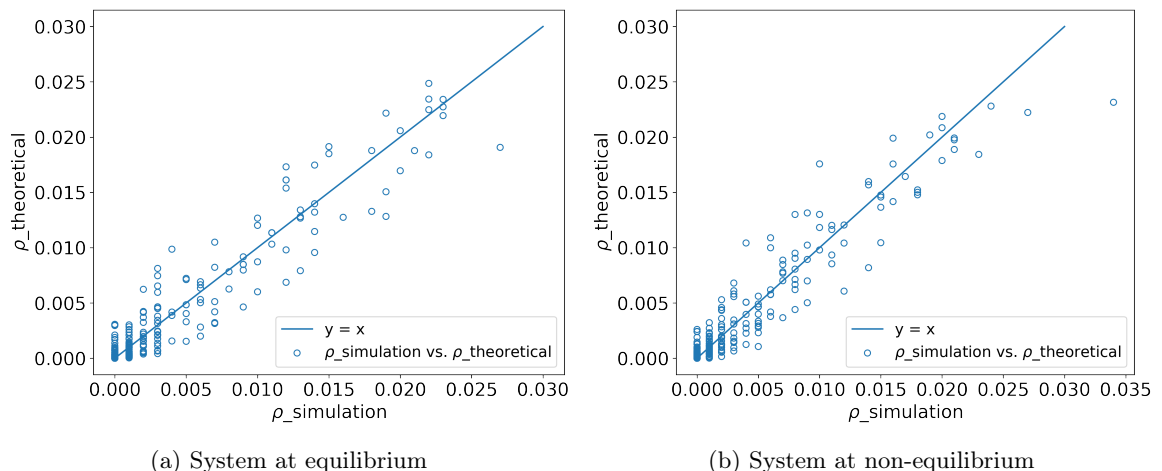


Figure 3.3: Plotting $p_{\text{simulation}}$ (results from numerical simulation) vs $p_{\text{theoretical}}$ (results from analytical solution) with an overlay plot of line $y = x$ with slope = 1 to check if the (a) numerical simulation results and (b) analytical solution results are in agreement.

Now, we start to quantitatively describe and compare equilibrium vs non-equilibrium systems by discussing our results for stochastic heat in Section 3.1.2, and the violation of FDT in Section 3.1.3.

3.1.2 Stochastic heat

In this section, we compare the average cumulative stochastic heat $\langle Q \rangle$ using Sekimoto's framework [20] between equilibrium and non-equilibrium systems.

Using Equation (2.21) and Equation (2.22) we obtain the stochastic heat for x_0 and x_1 , respectively. We compute for the average cumulative stochastic heat by taking the cumulative sum of δQ along each increment averaged over number of realizations. We use $T_0 = T_1$ to demonstrate a system at equilibrium, and $T_0 \neq T_1$ for non-equilibrium, having $a_{01} = a_{10}$.

Figure 3.4 shows that there is no heat flow ($\langle Q \rangle$ fluctuates around 0 for 1 realization) when the system is at equilibrium. In contrast, when $T_0 \neq T_1$, the system is not at equilibrium, and we observe a heat flow. For this example, we use $T_0 < T_1$, with $T_0 = 300K$ and $T_1 = 900K$. With this set-up, we observe a negative heat flow for x_0 , as we would expect since the particle x_0 is coupled to x_1 — with x_1 immersed in a heat bath T_1 that is hotter than x_0 's surrounding environment, T_0 . We recall that a negative heat flow corresponds to the energy flowing from the particle to the heat bath, following the convention used in Ref. [20]. Conversely, we observe a positive heat flow for x_1 , as we would expect since the particle x_1 is coupled to x_0 — with x_0 immersed in a heat bath T_0 that is colder than x_1 's surrounding environment, T_1 .

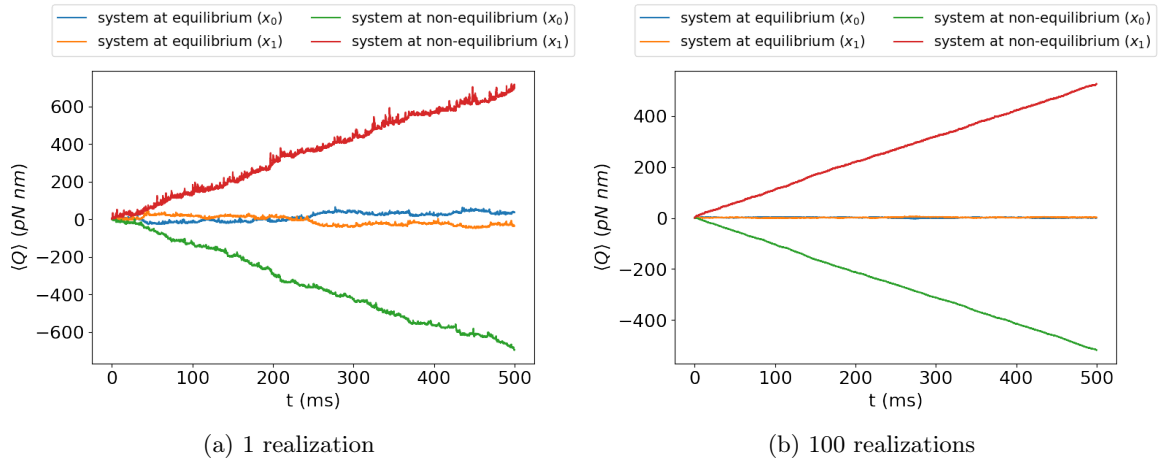


Figure 3.4: Average cumulative stochastic heat for a system at equilibrium and a system at non-equilibrium using Euler's numerical simulation scheme, with parameters: $a_{00} = a_{11} = -1$, $a_{01} = a_{10} = -0.5$, $k_B = 1.38 \cdot 10^{-2}$ pN nm, $\gamma_0 = \gamma_1 = 1$, with observation time = 500ms, for (a)1 realization, and (b)100 realizations. The system is at equilibrium when $T_0 = T_1 = 300K$, whereas a system is at non-equilibrium when $T_0 \neq T_1$, with $T_0 = 300K$, and $T_1 = 900K$.

Since the rate of energy dissipation is one of the most fundamental quantity to study non-equilibrium systems, after computing for the cumulative stochastic heat averaged over many realizations, we take an additional step of computing for the heat rate. As described in Chapter 2, we compute for the heat rate numerically by taking the slope of the average cumulative stochastic heat following Equation (2.23). We can also compute for the heat rate

analytically following Equation (2.24). We perform this method in the next few sections, as we describe the biophysical models.

3.1.3 Violation of Fluctuation-Dissipation Theorem

In this section, we discuss the quantification of the violation of the FDT – another method that is widely used to investigate non-equilibrium systems. We also present the results of the analytical derivation made for the Fourier-transformed autocorrelation function and response function with respect to the position.

As we have discussed in Chapter 2, the amount of energy dissipation is related to the violation function by the Harada-Sasa equality, given by:

$$\langle J \rangle = \int_{-\infty}^{+\infty} d\omega \tilde{h}(\omega)$$

where the violation function \tilde{h} is:

$$\tilde{h}(\omega) = \frac{\gamma}{2\pi} \left(\omega^2 \tilde{C}_x(\omega) - 2k_B T \omega \tilde{R}_x''(\omega) \right)$$

where \tilde{C}_x is the Fourier-transformed position autocorrelation function, and \tilde{R}_x'' is the imaginary part of the Fourier-transformed position response function, with the Fourier-transformation defined as: $\tilde{A}(\omega) = \int_{-\infty}^{+\infty} dt a(t) e^{i\omega t}$.

Derivation of the autocorrelation function and response function

We begin our analytical derivation of the autocorrelation and response functions for a 2-dimensional generic model described by an overdamped Markovian Langevin equation,

$$\begin{bmatrix} \gamma_0 & 0 \\ 0 & \gamma_1 \end{bmatrix} \begin{bmatrix} \dot{x}_0 \\ \dot{x}_1 \end{bmatrix} = \begin{bmatrix} a_{00} & a_{01} \\ a_{10} & a_{11} \end{bmatrix} \begin{bmatrix} x_0 \\ x_1 \end{bmatrix} + \begin{bmatrix} \xi_0 \\ \xi_1 \end{bmatrix} \quad (3.4)$$

x_0 describes the position, and is the variable that we are interested in. In this regard, we change our notation from \tilde{C}_x to \tilde{C}_{x_0} to refer as the Fourier-transformed position autocorrelation function, and from \tilde{R}_x'' to \tilde{R}_{x_0}'' to refer as the Fourier-transformed position response function, in the context of our 2-dimensional generic model.

Consequently, we can rewrite the violation function \tilde{h} as:

$$\tilde{h}(\omega) = \frac{\gamma}{2\pi} \left(\omega^2 \tilde{C}_{x_0}(\omega) - 2k_B T \omega \tilde{R}_{x_0}''(\omega) \right) \quad (3.5)$$

And the energy dissipated from the violation of FDT as:

$$\langle J \rangle = \gamma \int_{-\infty}^{+\infty} \frac{d\omega}{2\pi} \left(\omega^2 \tilde{C}_{x_0}(\omega) - 2k_B T \omega \tilde{R}_{x_0}''(\omega) \right) \quad (3.6)$$

A. Derivation of the autocorrelation function

The averaged autocorrelation function $\tilde{C}_{x_0}(\omega) = \langle \tilde{x}_0 \tilde{x}_0^* \rangle$ is given by the averaged product of \tilde{x}_0 with its complex conjugate \tilde{x}_0^* .

Using our generic model, we transform the two systems of equations in Equation (3.4) to Fourier space,

$$\begin{aligned} -i\omega\gamma_0\tilde{x}_0 &= a_{00}\tilde{x}_0 + a_{01}\tilde{x}_1 + \tilde{\xi}_0 \\ -i\omega\gamma_1\tilde{x}_1 &= a_{10}\tilde{x}_0 + a_{11}\tilde{x}_1 + \tilde{\xi}_1 \end{aligned}$$

Solving for \tilde{x}_0 , then we have:

$$\tilde{x}_0 = \frac{-a_{11}\tilde{\xi}_0 + a_{01}\tilde{\xi}_1 - i\omega\gamma_1\tilde{\xi}_0}{a_{11}a_{00} - a_{10}a_{01} + i\omega(\gamma_0a_{11} + \gamma_1a_{00}) - \omega^2\gamma_0\gamma_1}$$

We solve for the averaged autocorrelation function of position x_0 , $\tilde{C}_{x_0}(\omega) = \langle \tilde{x}_0 \tilde{x}_0^* \rangle$,

$$\tilde{C}_{x_0}(\omega) = \left\langle \frac{(a_{11}\tilde{\xi}_0 - a_{01}\tilde{\xi}_1)^2 + \omega^2\gamma_1^2\tilde{\xi}_0^2}{-2a_{11}a_{00}a_{10}a_{01} + a_{11}^2\omega^2\gamma_0^2 + (a_{10}a_{01} + \gamma_0\gamma_1\omega^2)^2 + a_{00}^2(a_{11}^2 + \omega^2\gamma_1^2)} \right\rangle \quad (3.7)$$

Having the following assumptions of our noise, with amplitude D_{x_0} and D_{x_1} :

$$\begin{aligned} \langle \xi_0(t)\xi_0(0) \rangle &= D_{x_0}\delta(t) \\ \langle \xi_1(t)\xi_1(0) \rangle &= D_{x_1}\delta(t) \\ \langle \xi_0\xi_1 \rangle &= 0 \end{aligned}$$

then we can simplify Equation 3.7 as:

$$\tilde{C}_{x_0}(\omega) = \frac{a_{11}^2D_{x_0} + a_{01}^2D_{x_1} + \omega^2\gamma_1^2D_{x_0}}{-2a_{11}a_{00}a_{10}a_{01} + a_{11}^2\omega^2\gamma_0^2 + (a_{10}a_{01} + \gamma_0\gamma_1\omega^2)^2 + a_{00}^2(a_{11}^2 + \omega^2\gamma_1^2)} \quad (3.8)$$

B. Derivation of the response function

We perturb the position coordinate x_0 with a δ -function in the time domain to obtain the response function, following Ref. [8].

$$\gamma_0\dot{x}_0 = a_{00}x_0 + a_{01}x_1 + \xi_0 + \delta(t) \quad (3.9)$$

$$\gamma_1\dot{x}_1 = a_{10}x_0 + a_{11}x_1 + \xi_1 \quad (3.10)$$

Transforming Equations 3.9 and 3.10 to Fourier space,

$$\begin{aligned} -i\omega\gamma_0\tilde{x}_0 &= a_{00}\tilde{x}_0 + a_{01}\tilde{x}_1 + \tilde{\xi}_0 + \tilde{\delta}(t) \\ -i\omega\gamma_1\tilde{x}_1 &= a_{10}\tilde{x}_0 + a_{11}\tilde{x}_1 + \tilde{\xi}_1 \end{aligned}$$

Since $\tilde{\delta}(t) = \int_{-\infty}^{\infty} \delta(t)e^{i\omega t}dt = 1$, then we have,

$$\begin{aligned} -i\omega\gamma_0\tilde{x}_0 &= a_{00}\tilde{x}_0 + a_{01}\tilde{x}_1 + \tilde{\xi}_0 + 1 \\ -i\omega\gamma_1\tilde{x}_1 &= a_{10}\tilde{x}_0 + a_{11}\tilde{x}_1 + \tilde{\xi}_1 \end{aligned}$$

Solving for \tilde{x}_0 , then we have:

$$\tilde{x}_0 = \frac{-a_{11}\tilde{\xi}_0 + a_{01}\tilde{\xi}_1 - i\omega\gamma_1\tilde{\xi}_0 - i\omega\gamma_1 - a_{11}}{a_{11}a_{00} - a_{10}a_{01} + i\omega(\gamma_0a_{11} + \gamma_1a_{00}) - \omega^2\gamma_0\gamma_1}$$

We solve for the averaged position,

$$\langle \tilde{x}_0 \rangle = \left\langle \frac{-a_{11}\tilde{\xi}_0 + a_{01}\tilde{\xi}_1 - i\omega\gamma_1\tilde{\xi}_0 - i\omega\gamma_1 - a_{11}}{a_{11}a_{00} - a_{10}a_{01} + i\omega(\gamma_0a_{11} + \gamma_1a_{00}) - \omega^2\gamma_0\gamma_1} \right\rangle$$

Since our noise is assumed to be Gaussian distributed with zero mean, $\langle \tilde{\xi}_0 \rangle = 0$, $\langle \tilde{\xi}_1 \rangle = 0$, then we have the averaged complex response of position x_0 (\tilde{R}_{x_0})

$$\tilde{R}_{x_0}(\omega) = \langle \tilde{x}_0 \rangle = \frac{-a_{11} - i\omega\gamma_1}{a_{11}a_{00} - a_{10}a_{01} + i\omega(\gamma_0a_{11} + \gamma_1a_{00}) - \omega^2\gamma_0\gamma_1} \quad (3.11)$$

With real part

$$\tilde{R}'_{x_0}(\omega) = \frac{a_{10}a_{01}a_{11} - a_{11}^2a_{00} - a_{00}\omega^2\gamma_1^2}{-2a_{11}a_{00}a_{10}a_{01} + a_{11}^2\omega^2\gamma_0^2 + (a_{10}a_{01} + \gamma_0\gamma_1\omega^2)^2 + a_{00}^2(a_{11}^2 + \omega^2\gamma_1^2)} \quad (3.12)$$

and imaginary part

$$\tilde{R}''_{x_0}(\omega) = \frac{\omega(a_{10}a_{01}\gamma_1 + a_{11}^2\gamma_0 + \gamma_0\gamma_1^2\omega^2)}{-2a_{11}a_{00}a_{10}a_{01} + a_{11}^2\omega^2\gamma_0^2 + (a_{10}a_{01} + \gamma_0\gamma_1\omega^2)^2 + a_{00}^2(a_{11}^2 + \omega^2\gamma_1^2)} \quad (3.13)$$

Using Equation (3.8) for $\tilde{C}_{x_0}(\omega)$, and Equation (3.13) for $\tilde{R}''_{x_0}(\omega)$, then we can calculate for the energy dissipation $\langle J \rangle$ Equation (3.6) from the FDT violation.

3.2 Non-reciprocal interactions: Biophysical Models

Since we have the concepts of stochastic heat, autocorrelation function, response function, and energy dissipation from FDT violation already laid out, in this section, we take two biophysical models that exhibit non-reciprocal interactions. The first biophysical model is a linear model of hair bundle oscillations [8], which exhibits non-reciprocal interactions. We take an additional step of comparing it to the same system but setting $a_{10} = a_{01} = 0$, and therefore uncoupled and in equilibrium. The second biophysical model is the cellular sensor model [15] which exhibits non-reciprocal interactions but is unidirectionally coupled.

3.2.1 Model 1: Hair bundle oscillations

We recall the linear model hair bundle oscillations as used in Ref. [8]. We refer to Chapter 2 for the discussion of the model.

$$\gamma\dot{x} = -kx + F + \eta_x \quad (3.14)$$

$$\lambda\dot{F} = -\bar{k}x - F + \eta_F \quad (3.15)$$

The dynamics of the position x of a hair bundle is governed by Equation (3.14), where γ is an effective drag coefficient, k a stiffness, and F an active driving force that is generated in the

bundle, and η the noise term that stems from the fluctuations of the thermal environment. Equation (3.15) describes the evolution of the active force F generated in the bundle, where λ is the relaxation time, \bar{k} is the coupling constant, and the noise term η_F that originates from the molecular motors having non-equilibrium fluctuations. η_x and η_F denote zero-mean, Gaussian white noises, with autocorrelation function $\langle \eta_x(t)\eta_x(0) \rangle = D_x\delta t$ (with amplitude D_x), and $\langle \eta_F(t)\eta_F(0) \rangle = D_F\delta t$ (with amplitude D_F). In addition, the two noise terms are uncorrelated with each other $\langle \eta_x\eta_F \rangle = 0$.

We recall that this model has non-reciprocal coupling with $1(a_{01}) \neq -k(a_{10})$, and therefore at non-equilibrium. In addition, we compare this with the same system but uncoupled (setting $a_{01} = a_{10} = 0$), and therefore at equilibrium. We proceed to investigate the characteristics of this system at two settings: equilibrium and non-equilibrium, and compare their differences.

We start by rewriting Equation (3.14) and Equation (3.15) in matrix form as

$$\begin{bmatrix} \gamma & 0 \\ 0 & \lambda \end{bmatrix} \begin{bmatrix} \dot{x} \\ \dot{F} \end{bmatrix} = \begin{bmatrix} -k & 1 \\ -\bar{k} & -1 \end{bmatrix} \begin{bmatrix} x \\ F \end{bmatrix} + \begin{bmatrix} \eta_x \\ \eta_F \end{bmatrix} \quad (3.16)$$

For the system at equilibrium, Equation (3.16) becomes

$$\begin{bmatrix} \gamma & 0 \\ 0 & \lambda \end{bmatrix} \begin{bmatrix} \dot{x} \\ \dot{F} \end{bmatrix} = \begin{bmatrix} -k & 0 \\ 0 & -1 \end{bmatrix} \begin{bmatrix} x \\ F \end{bmatrix} + \begin{bmatrix} \eta_x \\ \eta_F \end{bmatrix} \quad (3.17)$$

Equations (3.16), and (3.17) are now written in the same way as our 2-dimensional generic model. In this regard, we can compute for the stochastic heat and energy dissipation from violation of FDT in a straightforward manner.

Trajectories and Autocorrelation

We first check if we can distinguish between non-equilibrium and equilibrium systems by the behavior of their stochastic trajectories and autocorrelation. We simulate the stochastic trajectories of the position of the hair bundle x by using Equation (3.16) for the non-reciprocal system and (3.17) for the uncoupled system. This is shown in Figures 3.5(a) and 3.6(a), respectively. We use the values given in Table 3.1 with $k_B T = 4.1 \text{ pN} \cdot \text{nm}$. We also plot the corresponding autocorrelation in time domain ($C(\tau) = \langle x(t)x(t+\tau) \rangle$) in Figures 3.5(b) and 3.6(b).

Parameters	Values
k	$21 \cdot 10^{-3} \text{ pN} \cdot \text{nm}^{-1}$
\bar{k}	$1.348 \text{ pN} \cdot \text{nm}^{-1}$
γ	$8.72 \text{ pN} \cdot \text{ms} \cdot \text{nm}^{-1}$
λ	54.8 ms
D_x	$\sqrt{2k_B T \gamma} \text{ pN}^2 \cdot \text{ms}$
D_F	$\sqrt{4.916 \times 10^{-3}} \text{ pN}^2 \cdot \text{ms}$

Table 3.1: The parameters used in the linear model of hair bundle oscillations following Ref. [8]. With $k_B T = 4.1 \text{ pN nm}$, D_x and D_F are the noise strengths of η_x , and η_F , respectively.

We observe a striking difference between the behavior of the stochastic trajectories and autocorrelation function of the two systems: In Figure 3.5(a), the position of the bundle is stochastic and $x(t)$ oscillates in a passive manner because of thermal fluctuations. In contrast, oscillations of $x(t)$ in Figure 3.6(a) resembles sinusoidal waves, giving us a hint that

these oscillations are generated by active processes. In addition, the autocorrelation plot supports this claim with Figure 3.6(a) showing oscillations around 0 before it decays - a signature of non-equilibrium, whereas Figure 3.5(b) exponentially decays to 0.

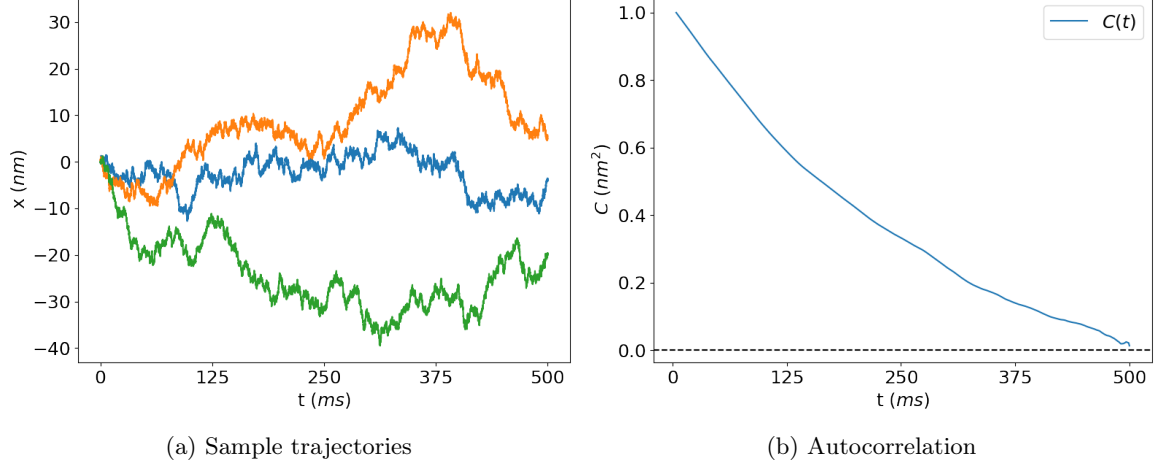


Figure 3.5: **Equilibrium:** (a) Three sample trajectories of the position of the hair bundle (in nm) as a function of time (in ms) using Euler numerical simulation scheme with simulation time step $\Delta t = 0.01\text{ms}$ and parameters given in Table 3.1, following the linear model described in Equation (3.16). (b) Corresponding normalized autocorrelation $\langle x(t)x(t + \tau) \rangle$ with values of τ from 1 up until the length of the trajectory with step size of 50, averaged over 100 realizations.

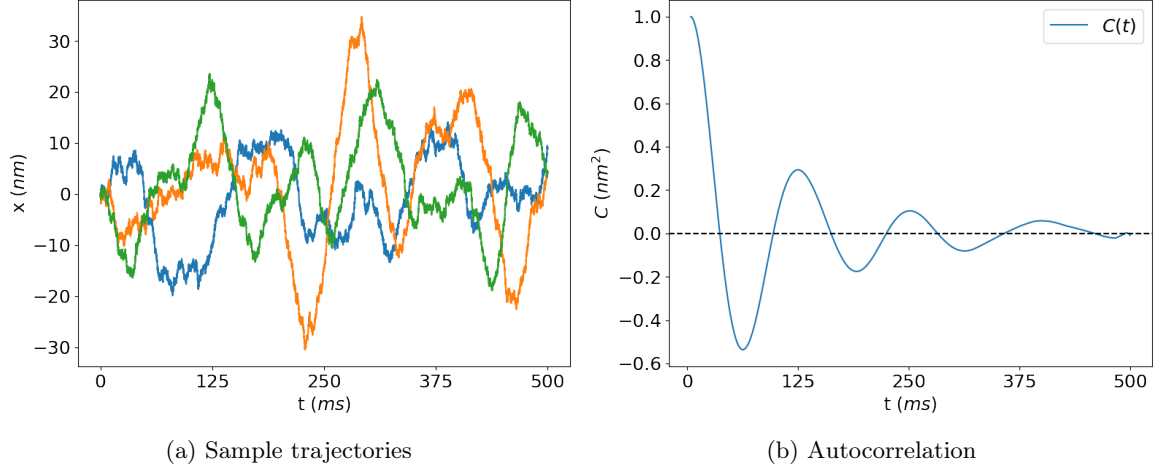


Figure 3.6: **Non-equilibrium:** (a) Three sample trajectories of the position of the hair bundle (in nm) as a function of time (in ms) using Euler numerical simulation scheme with simulation time step $\Delta t = 0.01\text{ms}$ and parameters given in Table 3.1, following the linear model described in Equation (3.17). (b) Corresponding normalized autocorrelation $\langle x(t)x(t + \tau) \rangle$ with values of τ from 1 up until the length of the trajectory with step size of 50, averaged over 100 realizations.

We now proceed with discussing our results for stochastic heat (Section 3.2.1A) from which we can calculate the heat rate $\langle \dot{Q} \rangle$, and, the violation of the FDT (Section 3.2.1B) from which we can calculate the energy dissipation $\langle J \rangle$. We recall that these two quantities tell us the amount of energy the system requires to keep away from equilibrium.

A. Stochastic Heat

In this section, we start by showing the cumulative stochastic heat of x and F averaged over 100 realizations, using Equation (2.21) and (2.22), respectively. We make a comparison between equilibrium and non-equilibrium systems.

Figure 3.7(a) shows that when our system is uncoupled, there is no heat flow. In contrast, when the system is at non-equilibrium, there is heat flow. This is in agreement with our results in Section 3.1.2. Further, we note that the heat flow for F is negative, this means that the energy is flowing from the particle to the heat bath following the convention used in Ref. [20].

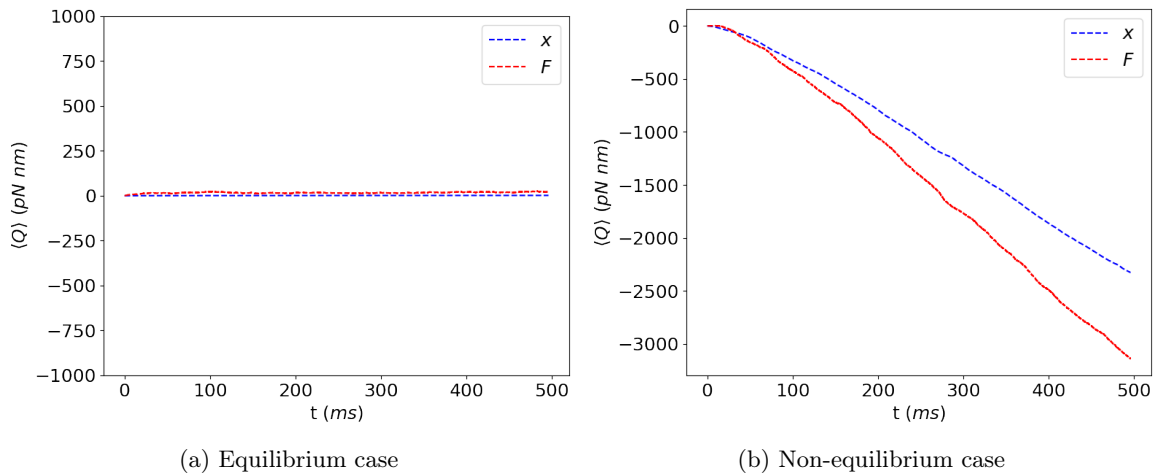


Figure 3.7: Cumulative stochastic heat of the position of the hair bundle x , and the active force F generated in the bundle (in pN nm) as a function of time (in ms) using Euler numerical simulation scheme averaged over 100 realizations, with simulation time step $\Delta t = 0.01\text{ms}$ and parameters given in Table 3.1 for (a)Equilibrium and (b)Non-equilibrium systems

We take the next step of quantifying for the heat rate. The heat rate is computed by taking the slope of the average cumulative stochastic heat. We present the results in Table 3.2. When the system is at equilibrium, heat rate is 0. When the system is not at equilibrium, there is a heat flow of 4.98 pN nm/ms for x and 6.72 pN nm/ms for F . We would like to compare if the heat rate of $x \langle \dot{Q}_x \rangle$ matches with the energy dissipation $\langle J \rangle$ calculated from the violation of FDT.

Heat rate	System at equilibrium	System at non-equilibrium
$\langle \dot{Q}_x \rangle$	0.00	4.98 pN nm/ms
$\langle \dot{Q}_F \rangle$	0.02	6.72 pN nm/ms
$\langle \dot{Q}_x \rangle + \langle \dot{Q}_F \rangle$	0.02	11.70 pN nm/ms

Table 3.2: Values of the heat rate computed by taking the slope of the average cumulative stochastic heat computed from Figure 3.7. Note that we take the $-\langle Q \rangle$ to match the convention used in the analytical solution of heat rate given in Equation (2.24).

B. Violation of Fluctuation-Dissipation Theorem

In this section, we show the plots of the autocorrelation and response functions using our analytical solution (Equation (3.8) and (3.13), respectively). In addition, we also compute for the autocorrelation function using numerical simulation (see details in appendix A). Afterwards, we compute for the rate of energy dissipation $\langle J \rangle$ computed from the violation of FDT using Harada-Sasa equality.

Autocorrelation Function

We observe that the autocorrelation function for an equilibrium system is peaked at zero frequency. When we take the log-log plot, the autocorrelation function has a shape of a Lorentzian function which is flat for low frequencies and has a ω^{-2} power law tail for high frequencies, as shown in Figure 3.8. This is in contrast with a non-equilibrium system where the autocorrelation function is peaked at a non-zero frequency, which is 8 Hz. This is the hair bundle's frequency of spontaneous oscillation [1]. This result is in agreement with the result from Berger, et.al [8]. When we take the log-log plot, we now observe that it doesn't have a Lorentzian shape. It has a flat shape at low frequencies, but then it peaks at a frequency near 8 Hz, and afterwards it does not follow a ω^{-2} power law tail for high frequencies, as shown in Figure 3.9.

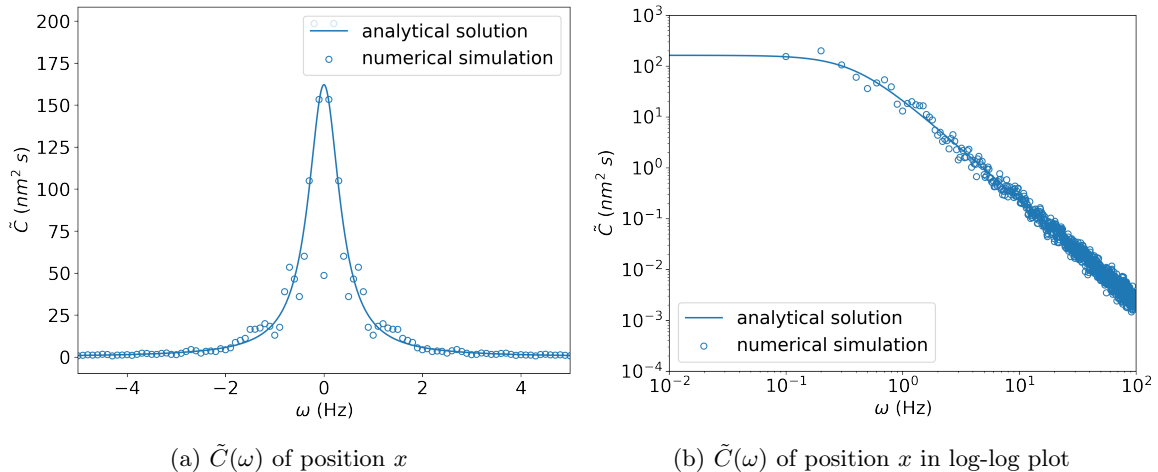


Figure 3.8: **Equilibrium:** (a) Plot of autocorrelation function of the hair bundle's position x using the analytical solution derived in Equation (3.8) using the parameters given in Table 3.1. (b) Autocorrelation function in a log-log plot using the same method as in (a). We overlay the results of the numerical simulation of duration $t = 100000s (\approx 28 \text{ hrs})$ using the same parameters given in Table 3.1. Details of computing this can be found in Appendix A. We use Equation (3.17) since the system is in equilibrium

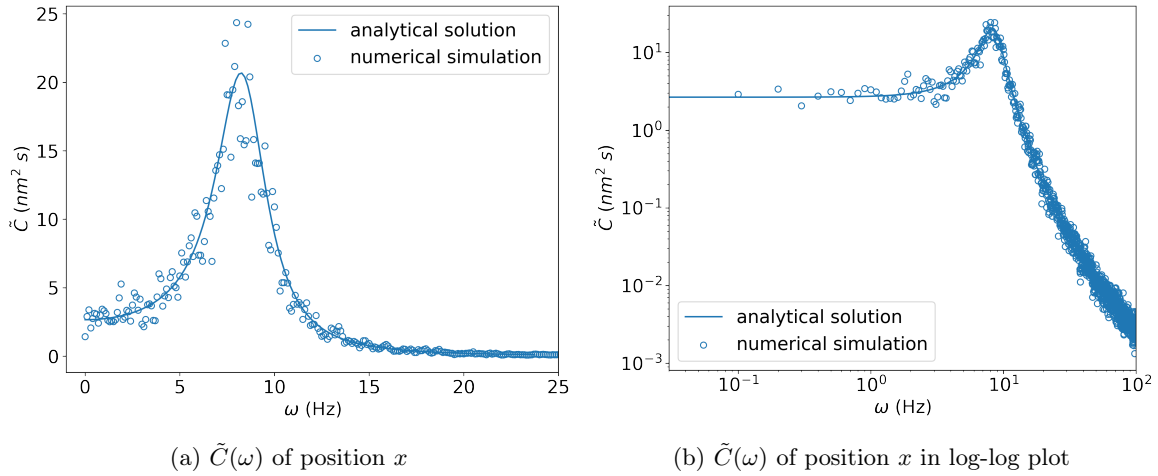


Figure 3.9: Non-equilibrium: (a) Plot of autocorrelation function of the hair bundle's position x using the analytical solution derived in Equation (3.8) using the parameters given in Table 3.1. (b) Autocorrelation function in a log-log plot using the same method as in (a). We overlay the results of the numerical simulation of duration $t = 100000$ s (≈ 28 hrs) using the same parameters given in Table 3.1. Details of computing this can be found in Appendix A. We use Equation (3.16) since the system is at non-equilibrium

Response function

Figure 3.10 shows the response functions for an equilibrium and non-equilibrium system. We first discuss the real part of the response function. For a non-equilibrium system, we observe that the response function peaks near 8 Hz, the frequency of spontaneous bundle oscillation, and then it starts to decline at a plateau for higher frequencies. We observe that for an equilibrium system, the peak of the response function is at 0 Hz.

The imaginary part of the response functions of the equilibrium system and non-equilibrium system have the same shape. The difference is that for a non-equilibrium system, the plot changes its sign at 8 Hz, whereas for an equilibrium system, the plot changes its sign at 0 Hz.

Our results of the response function for the non-equilibrium case agrees with the result of Berger, et.al [8].

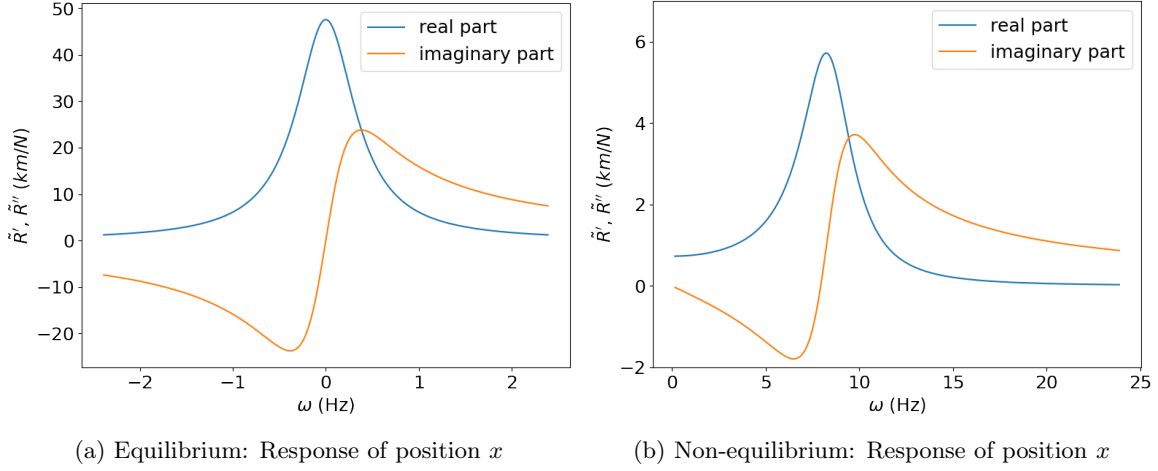


Figure 3.10: Plot of the response function of the hair bundle’s position x using the analytical solution derived in Equation (3.12) for the real part and Equation (3.13) for the imaginary part. We plot in (a) **Equilibrium** and in (b) **Non-equilibrium** systems using the parameters given in Table 3.1

Energy Dissipation from the Violation of the FDT

We recall the violation function given in Equation (3.5),

$$\tilde{h}(\omega) = \frac{\gamma}{2\pi} \left(\omega^2 \tilde{C}_{x_0}(\omega) - 2k_B T \omega \tilde{R}_{x_0}''(\omega) \right)$$

with $\tilde{C}_{x_0}(\omega)$ as the Fourier-transformed position autocorrelation function, and $\tilde{R}_{x_0}''(\omega)$ as the Fourier-transformed imaginary part of the response function. We also recall the energy dissipation given by Harada-Sasa equality as shown in Equation (3.18).

$$\langle J \rangle = \gamma \int_{-\infty}^{+\infty} \frac{d\omega}{2\pi} \left(\omega^2 \tilde{C}_{x_0}(\omega) - 2k_B T \omega \tilde{R}_{x_0}''(\omega) \right) \quad (3.18)$$

We can deduce that when

$$\tilde{C}_{x_0}(\omega) = \frac{2k_B T}{\omega} \tilde{R}_{x_0}''(\omega) \quad (3.19)$$

then the energy dissipation given by $\langle J \rangle$ is zero, which means that the system is in equilibrium. In contrast when this is not zero, then there is energy dissipation and is a signature for a non-equilibrium system.

We present in Figure 3.11 the plot of $\tilde{C}_{x_0}(\omega)$ and $\frac{2k_B T}{\omega} \tilde{R}_{x_0}''(\omega)$, and we immediately see that when the system is in equilibrium, the plots overlap each other completely, i.e., $\tilde{C}_{x_0}(\omega) = \frac{2k_B T}{\omega} \tilde{R}_{x_0}''(\omega)$ which obeys the FDT. For a non-equilibrium system, these two plots do not overlap each other, we see that $\tilde{C}_{x_0}(\omega)$ is largely greater than $\frac{2k_B T}{\omega} \tilde{R}_{x_0}''(\omega)$, thus FDT is violated. The system is out of equilibrium as a result of this FDT violation, which suggests the presence of an internal energy source.

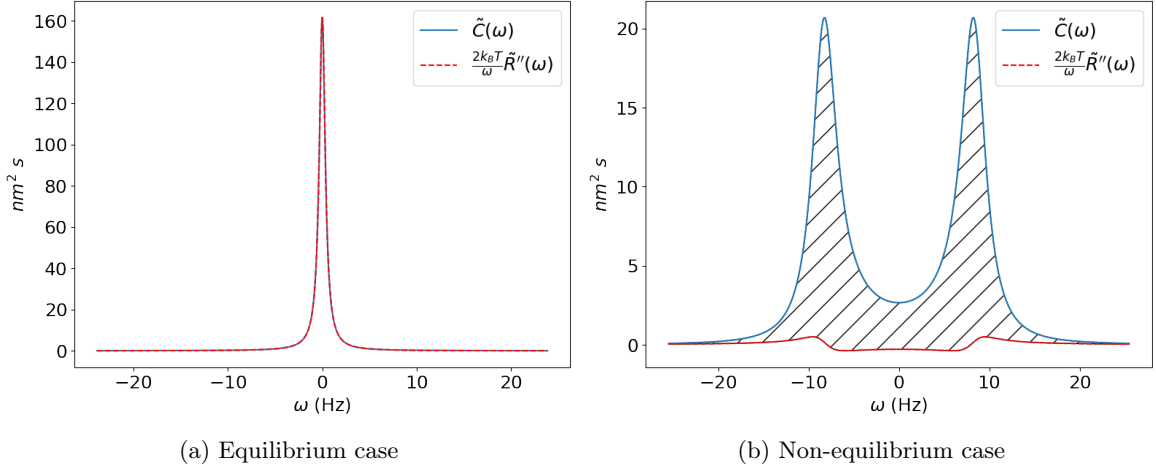


Figure 3.11: Plot of the hair bundle's position x : autocorrelation function, and imaginary part of the response function multiplied by a factor $\frac{2k_B T}{\omega}$. We use the analytical solution of $\tilde{C}_{x_0}(\omega)$ Equation (3.8) and $\tilde{R}_{x_0}''(\omega)$ Equation (3.13) that we have derived. We plot in (a) **Equilibrium** and in (b) **Non-equilibrium** systems using the parameters given in Table 3.1. The area between the two curves in (b) corresponds to the dissipation $\langle J \rangle$

We present in Figure 3.12 the plot of the violation function following Equation (3.5). We observe that the frequency that contributes the highest to the energy dissipation is at 8 Hz, the bundle's frequency of spontaneous oscillation.

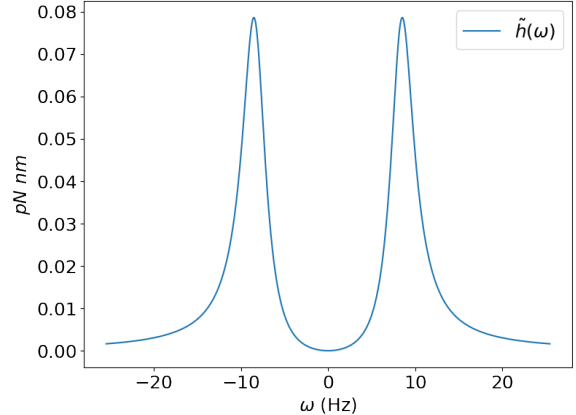


Figure 3.12: Plot of the violation function $\tilde{h}(\omega)$ as a function of ω as given in Equation (3.5) using the parameters given in Table 3.1

We solve for the energy dissipation $\langle J \rangle$ by taking the area between the two curves following Equation (3.18). We present our results in Table 3.3. For the equilibrium case, $\langle J \rangle = 0$ as what we would expect. For the non-equilibrium case, $\langle J \rangle = 4.97 \text{ pN nm/s}$. Energy dissipated is positive. This means that for this model, the energy is flowing from the system to the bath due to the active force generated by the molecular motors. The value we obtained for $\langle J \rangle$ is in close agreement with the results obtained from Berger, et.al [8] with $\langle J \rangle$ at 5.093 pN nm/ms.

Table 3.3: Energy dissipation for an equilibrium and non-equilibrium system following Equation (3.18).

System	Energy dissipation $\langle J \rangle$
Equilibrium	0
Non-equilibrium	4.97 pN nm/ms

We already discussed in Chapter 2 that for the case of 1-dimensional Langevin equation $\langle J \rangle = \langle \dot{Q} \rangle$. For a non-equilibrium system, we observed that our results for $\langle J \rangle$ agrees with our earlier results for $\langle \dot{Q}_x \rangle$, the heat rate from the position of the hair bundle. This means that for a non-reciprocal system, the value of $\langle J \rangle$ matches the heat flow of the degree of freedom that we have perturbed. We write again the values that we have obtained below:

System	Heat rate of x $\langle \dot{Q}_x \rangle$	Energy dissipation $\langle J \rangle$
Equilibrium	0	0
Non-equilibrium	4.98 pN nm/ms	4.97 pN nm/ms

Table 3.4: Values of $\langle \dot{Q}_x \rangle$ computed by taking the slope of the average cumulative stochastic heat computed from Figure 3.7, and energy dissipated from the violation of FDT $\langle J \rangle$ following Equation (3.18). The values of $\langle \dot{Q}_x \rangle$ and $\langle J \rangle$ are in close agreement.

Effective Temperature

We compute for the effective temperature from the autocorrelation function and response function, and compute for the ratio T_{EFF}/T given by Equation (3.20), at varying frequencies.

$$\frac{T_{EFF}(\omega)}{T} = \frac{\omega \tilde{C}_x(\omega)}{2k_B T \tilde{R}_x''(\omega)} \quad (3.20)$$

Figure 3.13(b) shows that for a non-equilibrium system, T_{EFF} departs from T at frequencies near 8 Hz, the bundle's frequency of spontaneous oscillation. In addition, the values changed its sign near 8 Hz, just like the plot of the imaginary part of the response function. This is in agreement with the results obtained by Martin, et.al [1].

We do not observe this behavior for the uncoupled system, i.e., the equilibrium system. Instead, Figure 3.13(a) shows that $T_{EFF}/T = 1$ at all frequencies. Therefore, thermal fluctuations were the cause of this hair bundle's spontaneous fluctuations [1].

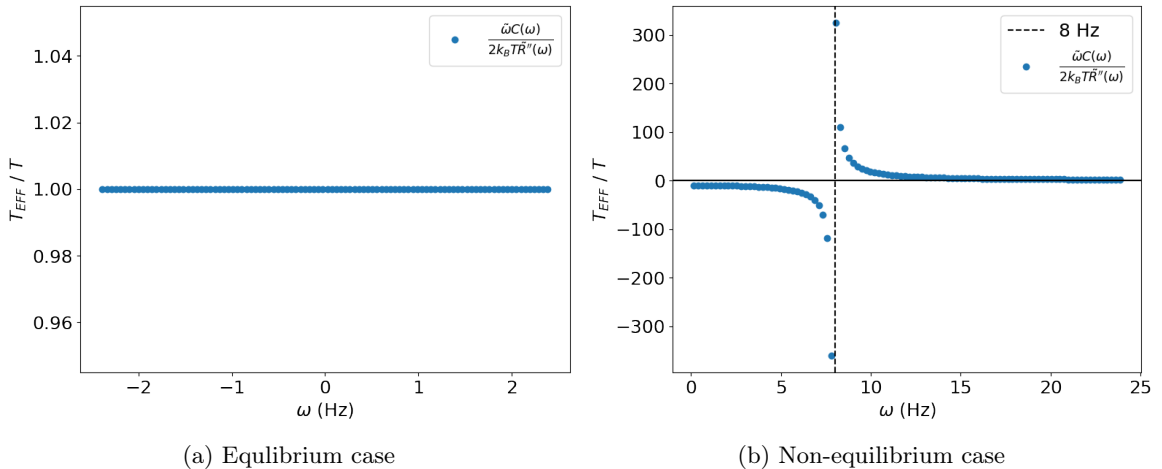


Figure 3.13: Plot of the ratio between T_{EFF}/T given in Equation (3.20). We plot in (a) **Equilibrium** and in (b) **Non-equilibrium** systems using the parameters given in Table 3.1

3.2.2 Model 2: Cellular sensor

In this section, we present our preliminary results for the second biophysical model exhibiting non-reciprocal interactions: cellular sensor. We recall the model as used in Ref. [15]. We refer to Chapter 2 for the discussion of the model.

$$\dot{r} = -\omega_r r + \omega_r x + \xi_r \quad (3.21)$$

$$\dot{x} = -\omega_x x + \xi_x \quad (3.22)$$

The sensor r which is related to the number of bound receptors is governed by Equation (3.21) where ω_r indicates the rate of binding to a ligand. The sensor measures the signal x which is the external ligand concentration, where ω_x indicates the rate of ligand concentration. ξ_r and ξ_x denote zero-mean, Gaussian white noises, with autocorrelation function $\langle \xi_i(t)\xi_j(t') \rangle = 2k_B T_j \gamma_j \delta_{ij} \delta(t - t')$.

In contrast to the hair bundle model that exhibits a bidirectional non-reciprocal coupling with $a_{01} \neq a_{10}$, the interaction between r and x is unidirectionally coupled, with the receptor (r) sensing the ligand (x), but not the other way around, hence $a_{10} = 0$, and also therefore at non-equilibrium. We now study how a non-reciprocal system with unidirectional coupling differs from that of a bidirectional coupling, and check its thermodynamic implications.

We start by rewriting Equation (3.21) and Equation (3.22) in matrix form as

$$\begin{bmatrix} \gamma_0 & 0 \\ 0 & \gamma_1 \end{bmatrix} \begin{bmatrix} \dot{r} \\ \dot{x} \end{bmatrix} = \begin{bmatrix} -\omega_r & \omega_r \\ 0 & -\omega_x \end{bmatrix} \begin{bmatrix} r \\ x \end{bmatrix} + \begin{bmatrix} \xi_r \\ \xi_x \end{bmatrix} \quad (3.23)$$

Equation (3.23) is now written in the same way as our 2-dimensional generic model. In this regard, we can compute for the stochastic heat and energy dissipation from violation of FDT in a straightforward manner.

Autocorrelation function and Response function

We first show the autocorrelation function and response function of our cellular sensor model following the parameters given in Table 3.5.

Parameters	Values
ω_r	$1 s^{-1}$
ω_x	$1 s^{-1}$
$\gamma_0 = \gamma_1$	1
D_r	$\sqrt{2k_B T \gamma_0}$
D_x	$\sqrt{2k_B T \gamma_1}$

Table 3.5: The parameters used in the cellular sensor model. With $k_B T = 4.1$ pN nm, D_r and D_x

are the noise strengths of ξ_r , and ξ_x , respectively.

Figure 3.14(a) shows that the autocorrelation function has a peak at 0 Hz. Figure 3.14(b) shows that the real part of the response function has a peak at 0 Hz, and that the imaginary part of the response function changes its sign at 0 Hz. The autocorrelation and response functions of this model looks similar to that of the equilibrium case of the hair bundle model earlier.

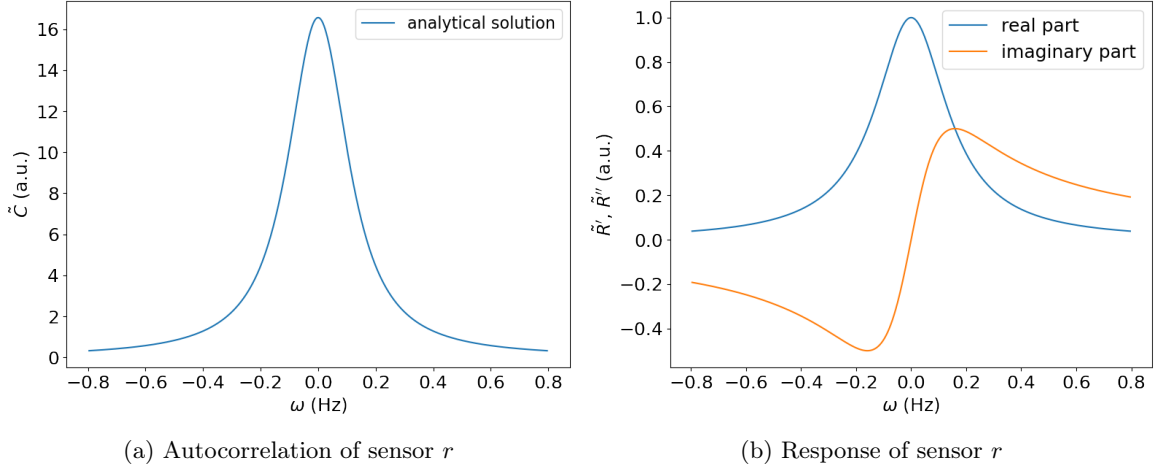
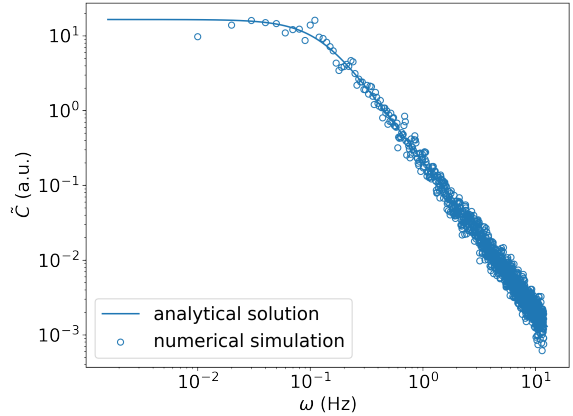


Figure 3.14: (a) Plot of the autocorrelation function (with arbitrary units - a.u.) of the sensor r using the analytical solution derived in Equation (3.8). (b) Plot of the response function (with arbitrary units - a.u.) of the sensor r using the analytical solution derived in Equation (3.12) for the real part and Equation (3.13) for the imaginary part. We use the parameters given in Table 3.5

When we take the log-log plot of the autocorrelation function as shown in Figure 3.15, it has a shape of a Lorentzian function which is flat for low frequencies and has a ω^{-2} power law tail for high frequencies. This makes us wonder if the system is truly at non-equilibrium, knowing that the autocorrelation and response function behaves similarly to the equilibrium case of the hair bundle model earlier. To answer this, we now turn to investigate if there is energy dissipation.

Figure 3.15: Autocorrelation function in a log-log plot (with arbitrary units - a.u.) using the analytical solution derived in Equation (3.8) using the parameters given in Table 3.5. We overlay the results of the numerical simulation of duration $t = 1000$ s and $\Delta_t = 0.001$ s



Heat Rate and Energy Dissipation from Violation of FDT

Figure 3.16(a) shows the cumulative stochastic heat of r and x averaged over 100 realizations, using Equations (2.21) and (2.22), respectively. We observe that there is no heat flow for x as it is uncoupled to r . In contrast, we observe a negative heat flow for r . Despite that the autocorrelation function and response function behaves similarly to the equilibrium system that we have observed for the hair bundle model, a net heat flow for r indicates that our cellular sensor model is at non-equilibrium.

We solve for the heat rate of r and x numerically (by taking the slope of the average cumulative stochastic heat), and analytically following Equation (2.24) for r , and Equation (2.25) for x .

We present in Figure 3.16(b) the plot of $\tilde{C}_{x_0}(\omega)$ and $\frac{2k_B T}{\omega} \tilde{R}_{x_0}''(\omega)$, and we immediately see that these two plots do not overlap each other. We see that $\tilde{C}_{x_0}(\omega)$ is largely greater than $\frac{2k_B T}{\omega} \tilde{R}_{x_0}''(\omega)$, thus FDT is violated.

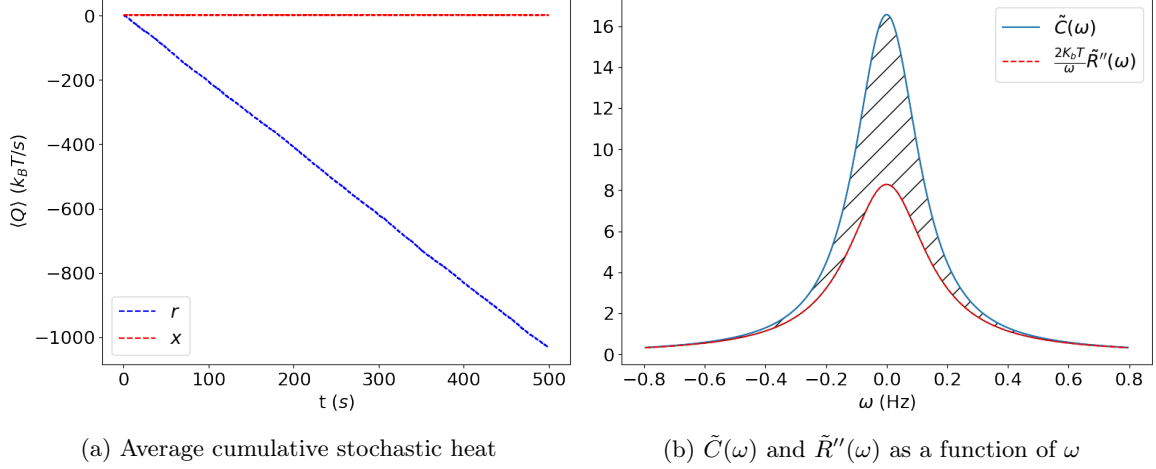
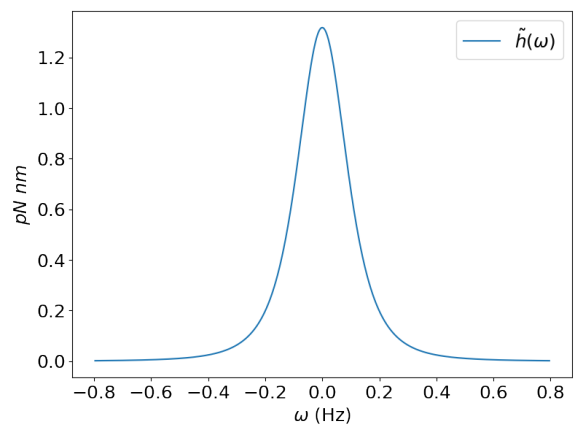


Figure 3.16: (a) Cumulative stochastic heat of the sensor r , and the signal (external ligand) x using Euler numerical simulation scheme averaged over 100 realizations, with simulation time step $\Delta t = 0.01$ s and parameters given in Table 3.5. (b) Plot of the sensor r : autocorrelation function, and imaginary part of the response function multiplied by a factor $\frac{2k_B T}{\omega}$. We use the analytical solution of $\tilde{C}(\omega)$ Equation (3.8) and $\tilde{R}''(\omega)$ Equation (3.13) that we have derived. We use the parameters given in Table 3.5. The area between the two curves in (b) corresponds to the dissipation $\langle J \rangle$

We present in Figure 3.17 the plot of the violation function following Equation (3.5). The frequency that contributes the highest to the energy dissipation is at 0 Hz.

Figure 3.17: Plot of the violation function $\tilde{h}(\omega)$ as a function of ω as given in Equation (3.5) using the parameters given in Table 3.5



We present in Table 3.6 the values of heat rate (from the analytical solution and numerical simulation), and energy dissipated from the violation of FDT $\langle J \rangle$. We observe that these quantities are 0 for x , as what we would expect since it is uncoupled to r . However, r has

a non-zero value for $\langle J \rangle$ and $\langle \dot{Q} \rangle$. Energy dissipated is positive for this model. This means that energy is flowing from the system to the bath due to the action of the external agent – in this case, the binding and unbinding of ligands at different concentrations [15]. We again observe that $\langle J \rangle = \langle \dot{Q}_r \rangle$, the heat flow of the degree of freedom that we have perturbed.

Parameters	$\langle \dot{Q} \rangle$ (numerical simulation)	$\langle \dot{Q} \rangle$ (analytical solution)	$\langle J \rangle$
r	$2.08 \text{ } k_B T/\text{s}$	$2.07 \text{ } k_B T/\text{s}$	$2.07 \text{ } k_B T/\text{s}$
x	0.00	0.00	-

Table 3.6: Values of the heat rate of r and x from numerical simulation (by taking the slope of the average cumulative stochastic heat from Figure 3.7), and analytically following Equation (2.24) for r , and Equation (2.25) for x . We note that for the numerical simulation, we take $-\langle \dot{Q} \rangle$ to match the convention used in our analytical solution. We also show the value of $\langle J \rangle$ following Equation (3.18)

Effective Temperature

We compute for the effective temperature from the autocorrelation function and response function, and compute for the ratio T_{EFF}/T given by Equation (3.20), at varying frequencies. We recall that for an equilibrium system, $T_{EFF}/T = 1$ [1] which we have also shown in our earlier results (see Figure 3.13). However, our figure below shows that T_{EFF} departs from T at frequencies near 0 Hz. This tells us that our system is at non-equilibrium.

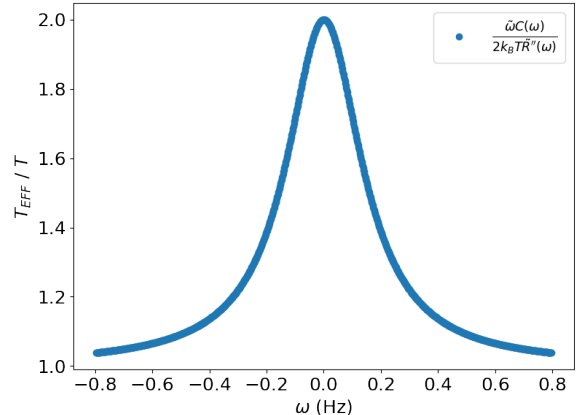


Figure 3.18: Plot of the ratio T_{EFF}/T as a function of ω given in Equation (3.20) using the parameters given in Table 3.5

3.3 Non-reciprocal Interactions: Different Degrees of Reciprocity

In this section we show that systems with non-reciprocal interactions in general violate the FDT, and are associated with net energy dissipation. As mentioned in Chapter 2, several quantities have been established to measure the distance from equilibrium of system, and to estimate the energy the system needs to keep away from equilibrium:

- Energy dissipated $\langle J \rangle$ of x_0 quantified using Harada-Sasa equality[8, 10] Equation (3.18) which measures the degree of violation of FDT
- Heat rate of $x_0 \langle \dot{Q}_0 \rangle$, and $x_1 \langle \dot{Q}_1 \rangle$ given in Equation (2.23) calculated by taking the slope of its respective average cumulative stochastic heat using Sekimoto's framework

[20] which measures the energy dissipated by the particle to the heat bath. We also compute for the heat rate using the analytical solution given in Equation (2.24, 2.25), and

- Total entropy production rate [11] (total EPR) as given in Equation(2.26).

Using these 3 quantities, we now turn to investigate what happens when we vary the degree of reciprocity, or tune the interactions between two systems. Again, we use the 2-dimensional model below:

$$\begin{aligned}\gamma_0 \dot{x}_0 &= a_{00}x_0 + a_{01}x_1 + \sqrt{2k_B T_0} \xi_0 \\ \gamma_1 \dot{x}_1 &= a_{10}x_0 + a_{11}x_1 + \sqrt{2k_B T_1} \xi_1\end{aligned}$$

We discuss in 3.3.1 the behavior of these 3 quantities for varying values of a_{01} when we have isothermal conditions, $T_0 = T_1$. We discuss in 3.3.2 the behavior of the estimated energy from the violation of FDT $\langle J \rangle$ and the heat rate for non-isothermal conditions.

3.3.1 Isothermal conditions, $T_0 = T_1$

Figure 3.19 shows $\langle J \rangle$, heat rate, and total EPR against different values of a_{01} , given the following parameters: $\gamma_0 = \gamma_1 = 1$, $T_0 = T_1 = 300K$, $a_{00} = a_{11} = -1$, and $a_{10} = -0.5$. As a first observation, Figure 3.19(a) shows that the energy dissipated from the violation of FDT $\langle J \rangle$, and the heat rate of $x_0 \langle \dot{Q}_0 \rangle$ are in excellent agreement with each other.

Let us discuss the behavior of these quantities with the following cases:

Case 1: When $a_{01} = -0.5$, the system is:

$$\dot{x}_0 = -x_0 - 0.5x_1 + \sqrt{2k_B T_0} \xi_0 \quad (3.24)$$

$$\dot{x}_1 = -0.5x_0 - x_1 + \sqrt{2k_B T_1} \xi_1 \quad (3.25)$$

Since $a_{10} = a_{01}$, then the coupling is reciprocal, which indicates that the system is in equilibrium and obeys the FDT. With the system in equilibrium, then $\langle J \rangle$ (Figure 3.19(a)), heat rate (Figure 3.19(b) and (c)), and total EPR (Figure 3.19(d)) are all zero.

Case 2: When $a_{01} = 0$, the system becomes:

$$\dot{x}_0 = -x_0 + \sqrt{2k_B T_0} \xi_0 \quad (3.26)$$

$$\dot{x}_1 = -0.5x_0 - x_1 + \sqrt{2k_B T_1} \xi_1 \quad (3.27)$$

The system x_0 is in equilibrium since it is uncoupled to x_1 , as shown in Equation (3.26). With the system in equilibrium, Figure 3.19(a) and (b) show that the values of $\langle J \rangle$ and heat rate of x_0 are zero.

In contrast, the system x_1 is unidirectionally coupled to x_0 , as shown in Equation (3.27). As discussed in Chapter 2, systems with unidirectional coupling are non-equilibrium models, as a result, heat rate of x_1 is non-zero and positive as shown in Figure 3.19(c). This indicates that heat is dissipated from the particle to the heat bath. As a consequence, the total EPR

is also non-zero.

Case 3: When $-0.5 < a_{01} < 0$, the system follows Equation (3.24) and Equation (3.25) with $a_{01} \neq a_{10}$.

When $a_{01} \neq a_{10}$, and $a_{10}T_0 \neq a_{01}T_1$ then the system has non-reciprocal coupling and is not in equilibrium. As a result, $\langle J \rangle$, heat rate and total EPR are all non-zero – with $\langle \dot{Q}_0 \rangle$ and $\langle J \rangle$ that are negative, and $\langle \dot{Q}_1 \rangle$ and total EPR that are positive.

With this intuition, then the values of $\langle \dot{Q}_0 \rangle$ and $\langle J \rangle$ from $-0.5 < a_{01} < 0$ should have a parabolic shape. We can observe that these two plots are symmetric, and the value of a_{01} in which $\langle \dot{Q}_0 \rangle$ and $\langle J \rangle$ is at minimum can be calculated as:

$$a_{01} = 0.5 \left(a_{10} \frac{T_0}{T_1} \right) \quad (3.28)$$

Using Equation (3.28) and with $a_{10} = -0.5$, then the value of a_{01} at which $\langle \dot{Q}_0 \rangle$ and $\langle J \rangle$ is minimum is at $a_{01} = -0.25$. This is observed in Figure 3.19(a) and (b).

We also observe that the plot of $\langle \dot{Q}_1 \rangle$ in Figure 3.19(c) increases linearly as a_{01} increases from -0.5 to 0 . We observe the following:

- At $a_{01} = 0$, $\langle \dot{Q}_1 \rangle = 0.5$ which is the maximum. This is because x_1 is unidirectionally coupled to x_0 , indicating non-equilibrium.
- At $a_{01} = -0.5$, $\langle \dot{Q}_1 \rangle = 0$ which is the minimum. This is because x_0 and x_1 have reciprocal coupling, indicating equilibrium.

As a result, the total EPR also increases as a_{01} increases from -0.5 to 0 , although not linearly.

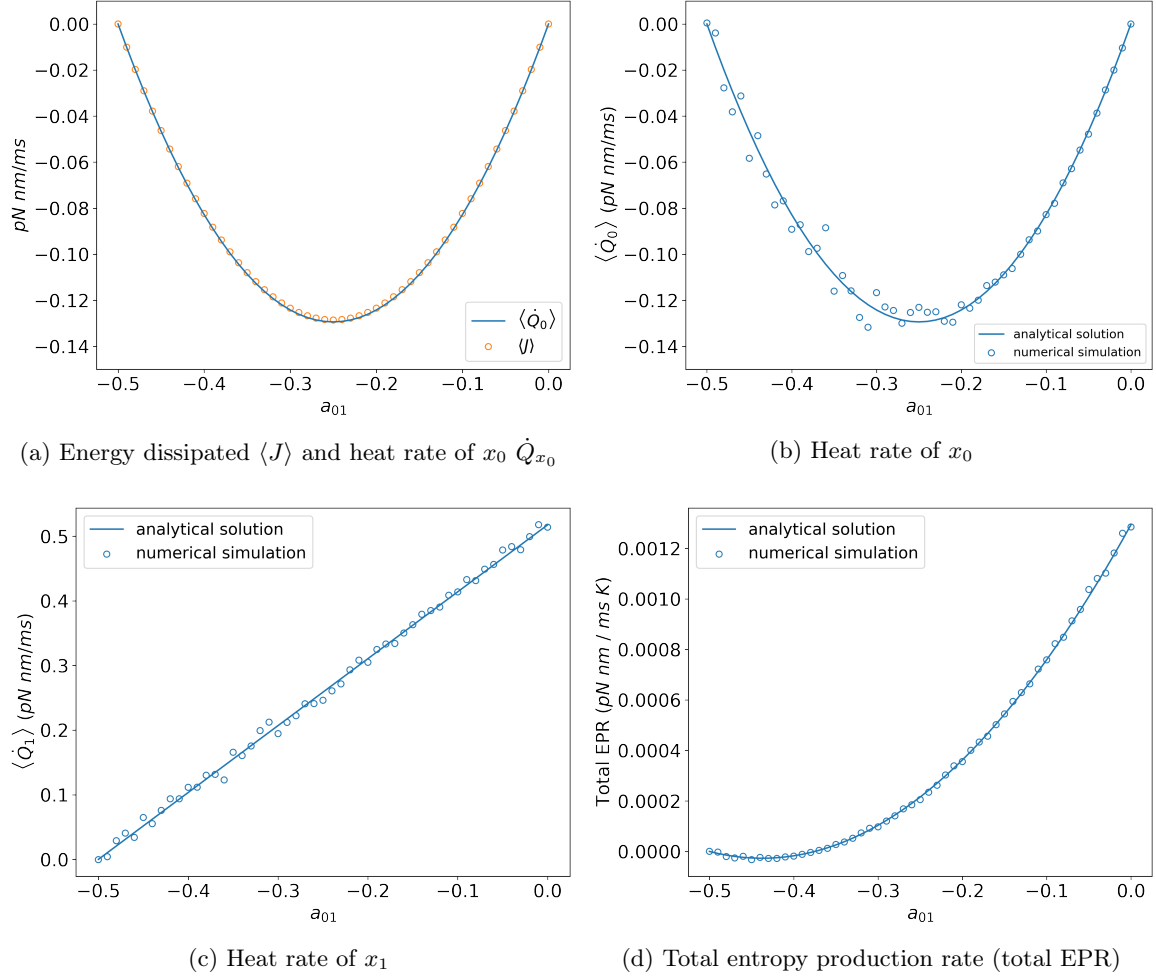


Figure 3.19: Different quantities used to measure the degree of non-equilibrium in a 2-dimensional model plotted against the different values of a_{01} : (a) Energy dissipated, $\langle J \rangle$ (circles) of x_0 from the violation of FDT given by Equation (3.18). We overlay the results of the analytical solution of heat rate $\langle \dot{Q}_0 \rangle$ following Equation (2.24). (b and c) Heat rate of x_0 and x_1 with the analytical solution (lines) following Equation (2.24, 2.25), and numerical simulation (circles) following Equation (2.23). (d) Total entropy production rate with the analytical solution (lines) and numerical simulation (circles) given by Equation (2.26). The other parameters used are: $a_{00} = a_{11} = -1$, $a_{10} = -0.5$, $T_0 = T_1 = 300K$, $k_B = 1.38 \cdot 10^{-2}$ pN nm. The numerical simulation is performed for a duration of $t = 800s$ with $\Delta t = 0.01s$ averaged over 100 realizations

3.3.2 Non-isothermal conditions

Figure 3.20 shows the estimated energy dissipation from violation of FDT $\langle J \rangle$, and the heat rate of x_0 $\langle \dot{Q}_0 \rangle$, calculated analytically, with $a_{10} = -0.5$ and $T_0 = 300K$ plotted against different values of a_{01} and T_1 . We show the results of $\langle \dot{Q}_0 \rangle$ computed using the analytical solution and numerical simulation in Figure 3.21.

We observe the following:

1. The values of $\langle J \rangle$ and $\langle \dot{Q}_0 \rangle$ are in excellent agreement with each other for varying values of T_1 .
2. When $T_0 = T_1$, the value of a_{01} at which $\langle J \rangle$ and $\langle \dot{Q}_0 \rangle$ are minimum is at $a_{01} = -0.25$, as we have shown in our earlier results. When $T_0 \neq T_1$, the value of a_{01} at which $\langle J \rangle$ and $\langle \dot{Q}_0 \rangle$ are minimum is $a_{01} \neq -0.25$ and varies as T_1 varies. We still observe that these plots are symmetric with respect to the point of a_{01} following Equation (3.28).
3. When $a_{01} = 0$, $\langle J \rangle$ and $\langle \dot{Q}_0 \rangle$ are both zero for varying values of T_1 , since this entails that x_0 is uncoupled and indicates equilibrium. This is in agreement with our earlier results.
4. When $a_{01} = -0.5$, the value of $\langle J \rangle$ and $\langle \dot{Q}_0 \rangle$ are non-zero and vary as $T_0 \neq T_1$. We expect these values to be non-zero as $a_{10}T_0 \neq a_{01}T_1$, which indicates non-equilibrium [11]. In addition, when $T_1 < T_0$, the values of $\langle J \rangle$ and heat rate are negative, with the energy flowing from the bath to the system. Whereas, when $T_1 > T_0$, the energy is flowing from the system to the bath, and so the values of $\langle J \rangle$ and heat rate are positive.

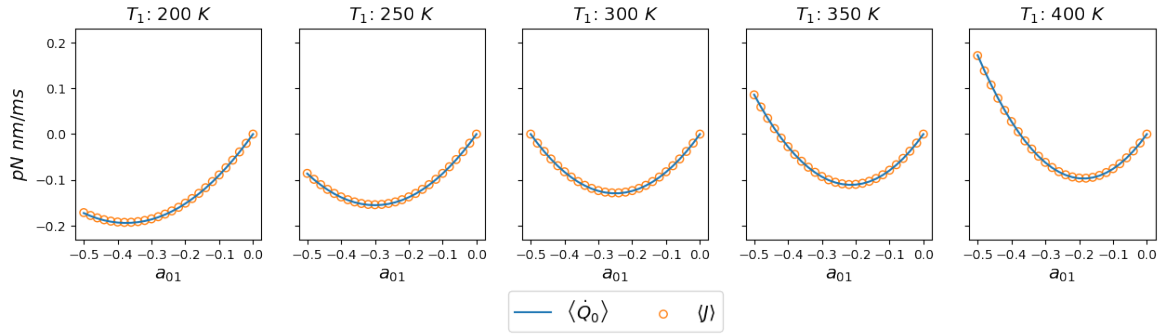


Figure 3.20: Energy dissipated from the violation of FDT $\langle J \rangle$ (circles) plotted against varying values of a_{01} , and T_1 given in Equation (3.6). We overlay the results of the analytical solution of heat rate $\langle \dot{Q}_0 \rangle$ (lines) following Equation (2.24). The parameters used are: $a_{00} = a_{11} = -1$, $a_{10} = -0.5$, $T_0 = 300K$, $k_B = 1.38 \cdot 10^{-2}$ pN nm

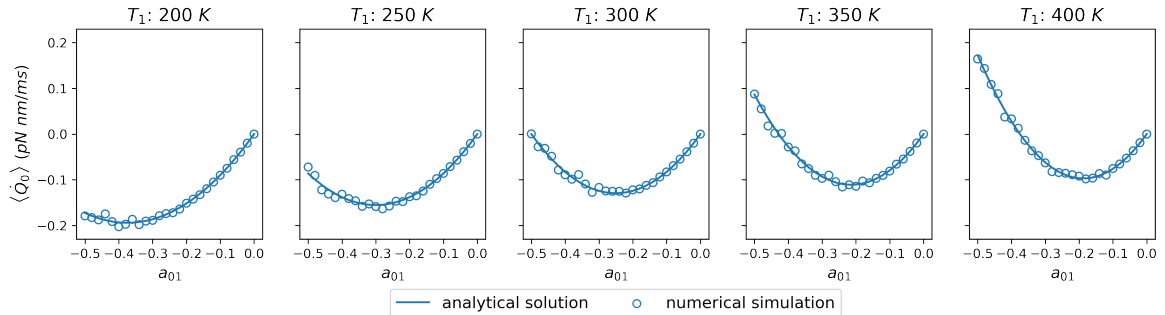


Figure 3.21: Heat rate of x_0 with the analytical solution (lines) following Equation (2.24), and numerical simulation (circles) following Equation (2.23) plotted against varying values of a_{01} , and T_1 . The parameters used are: $a_{00} = a_{11} = -1$, $a_{10} = -0.5$, $T_0 = 300K$, $k_B = 1.38 \cdot 10^{-2}$ pN nm

CHAPTER 4

Conclusions

In this work, we have studied from a thermodynamic perspective the behavior and characteristics of (biophysical) models that exhibit non-reciprocal interactions. These non-reciprocal interactions between two systems appear as non-conservative forces which drive the system away from equilibrium. The violation of the fluctuation-dissipation theorem (FDT) and a finite net energy flow demonstrate this non-equilibrium property. To estimate the energy that the system needs to keep away from equilibrium, we computed $\langle J \rangle$ using the Harada-Sasa equality which relates the energy dissipated to the extent of violation of the FDT, and the heat rate $\langle \dot{Q} \rangle$ found by taking the slope of the average cumulative stochastic heat using Sekimoto's framework. We have shown that for a system with non-reciprocal interactions, the value of $\langle J \rangle$ matches the heat flow $\langle \dot{Q}_0 \rangle$ of the degree of freedom that we have perturbed.

As concrete examples, we studied two biophysical models, namely, a hair bundle model and a cellular sensor model. In the hair bundle model, the position of the hair bundle (x_0) and the active force generated by the molecular motors (x_1) are non-reciprocally coupled, with coupling strengths $a_{01} \neq a_{10}$. We have shown that the autocorrelation function has a peak at 8 Hz, the bundle's frequency of spontaneous oscillation. We have also shown that the magnitude of position fluctuations ($\tilde{C}_{x_0}(\omega)$) is largely greater than the linear response to external stimuli ($\frac{2k_B T}{\omega} \tilde{R}_{x_0}''(\omega)$), thus FDT is violated. The system is out of equilibrium as signaled by this FDT violation, which suggests the presence of an internal energy source. The frequency that contributes the highest to the energy dissipation is at 8 Hz. Our computations showed that $\langle J \rangle$ and $\langle \dot{Q}_{x_0} \rangle \approx 4.98 \text{ pN nm/ms}$. This is in close agreement with the results from Berger, et.al [8], with $\langle J \rangle$ at 5.093 pN nm/ms. Energy dissipated is positive for this model. This means that energy is flowing from the system to the bath due to the active force generated by the molecular motors. Our results of the ratio T_{EFF}/T as a function of ω shows that T_{EFF}/T departs from 1 at 8Hz, this is in agreement with the results of Martin, et.al [1].

In addition, we compared this model to the same system but setting $a_{01} = a_{10} = 0$, where the system is uncoupled and therefore at equilibrium. As expected, $\tilde{C}_{x_0}(\omega) = \frac{2k_B T}{\omega} \tilde{R}_{x_0}''(\omega)$ which obeys the FDT. There is no net energy flow with $\langle J \rangle = \langle \dot{Q}_{x_0} \rangle = 0$. Consequently, the ratio $T_{EFF}/T = 1$ at all frequencies.

In the cellular sensor model, the sensor which is related to the number of bound receptors measures the signal, which is the external ligand concentration. In contrast to the hair bundle model that exhibits a bidirectional non-reciprocal coupling with $a_{01} \neq a_{10}$, the interaction between the sensor (x_0) and the signal (x_1) is unidirectionally coupled, with the receptor sensing the ligand, but not the other way around, hence $a_{10} = 0$. This unidirectionally cou-

pling also brings the system away from equilibrium. Our preliminary results showed that the autocorrelation function has a peak at 0 Hz. The FDT is also violated with $\tilde{C}_{x_0}(\omega)$ largely greater than $\frac{2k_B T}{\omega} \tilde{R}_{x_0}''(\omega)$. The frequency that contributes the highest to the energy dissipation is at 0 Hz. Our computations showed that $\langle J \rangle$ and $\langle \dot{Q}_{x_0} \rangle$ are around 2.07 pN nm/ms. Energy dissipated is positive for this model. This means that energy is flowing from the system to the bath due to the action of the external agent – in this case, the binding and unbinding of ligands at different concentrations [15]. Our results of the ratio T_{EFF}/T as a function of ω shows that T_{EFF}/T departs from 1 at 0 Hz.

Finally, we investigated what happens when we vary the degree of reciprocity, or tune the interactions between two systems. We keep $a_{10} = -0.5$, but varied a_{10} from -0.5 to 0. We have shown that for isothermal and non-isothermal conditions, $\langle J \rangle$, and heat rate of x_0 are symmetric and follows a parabolic shape with the minimum energy at $a_{01} = 0.5 \left(a_{10} \frac{T_0}{T_1} \right)$. We have shown that in the presence of temperature gradients, two systems with bidirectional non-reciprocal coupling can still reach equilibrium as long as $a_{10}T_0 = a_{01}T_1$ following Loos, et.al [11]. In this case, we do not observe a net energy dissipation. Whereas a system with unidirectionally coupling cannot reach an equilibrium state, and we observed a net energy dissipation.

In this final two paragraphs, we discuss future works and open questions as possible lines of research for the future:

Future work:

- We have shown the contour plots of the joint PDF of x_0 and x_1 , in addition, we can overlay quiver plots to show the fluxes.
- As we have only performed the numerical simulation of the autocorrelation function numerically, we can also perform the numerical simulation of the response function. Experimentally, a sinusoidal force (e.g. $A \cos(\omega t)$) is applied to the system at varying ω from which we can sample some values of ω of the response function. Berger, et.al [8] in their theoretical approach applied a white noise perturbation force which has components throughout the omega-spectrum - which can be done in simulations. To perform a numerical simulation of the response function, we can apply a Gaussian-white-noise force to x , the position of the hair bundle and check the results.
- The parameters used for the cellular sensor model are not from a physical origin, as there are no parameters found in the literature. We can continue studying the model and try other parameters, to see if the dynamics change.

Open questions:

- How general is our key result that $\langle J \rangle = \langle \dot{Q}_0 \rangle$?
- With our preliminary results of the cellular sensor model, can we extend our model by considering the response of the sensor to concentration changes of the ligand?
- Aside from the relationship between the energy dissipated and the violation of FDT, can we also infer a relation between the violation of FDT and the efficiency? Efficiency from the cellular sensor model [15] is defined as the relationship between the rate with which the sensor learns about the signal, and the energy dissipated by the sensor.

Bibliography

- [1] P. Martin, A. Hudspeth, and F. Jülicher, “Comparison of a hair bundle’s spontaneous oscillations with its response to mechanical stimulation reveals the underlying active process,” *Proceedings of the National Academy of Sciences*, vol. 98, no. 25, pp. 14 380–14 385, 2001.
- [2] H. Turlier, D. A. Fedosov, B. Audoly, T. Auth, N. S. Gov, C. Sykes, J.-F. Joanny, G. Gompper, and T. Betz, “Equilibrium physics breakdown reveals the active nature of red blood cell flickering,” *Nature physics*, vol. 12, no. 5, pp. 513–519, 2016.
- [3] É. Fodor, C. Nardini, M. E. Cates, J. Tailleur, P. Visco, and F. Van Wijland, “How far from equilibrium is active matter?” *Physical review letters*, vol. 117, no. 3, p. 038103, 2016.
- [4] S. J. Blundell and K. M. Blundell, *Concepts in thermal physics*. Oxford University Press on Demand, 2010.
- [5] B. Alberts, D. Bray, K. Hopkin, A. D. Johnson, J. Lewis, M. Raff, K. Roberts, and P. Walter, *Essential cell biology*. Garland Science, 2015.
- [6] F. Flaticon, “birds icons,” 2022. [Online]. Available: <https://www.flaticon.com/free-icons/birds>
- [7] S. A. Loos, *Stochastic Systems with Time Delay: Probabilistic and Thermodynamic Descriptions of Non-Markovian Processes Far from Equilibrium*. Springer Nature, 2021.
- [8] F. Berger and A. Hudspeth, “Violation of the fluctuation-response relation from a linear model of hair bundle oscillations,” *bioRxiv*, 2022.
- [9] É. Fodor, W. W. Ahmed, M. Almonacid, M. Bussonnier, N. S. Gov, M.-H. Verlhac, T. Betz, P. Visco, and F. van Wijland, “Nonequilibrium dissipation in living oocytes,” *EPL (Europhysics Letters)*, vol. 116, no. 3, p. 30008, 2016.
- [10] T. Harada and S.-i. Sasa, “Equality connecting energy dissipation with a violation of the fluctuation-response relation,” *Physical review letters*, vol. 95, no. 13, p. 130602, 2005.
- [11] S. A. Loos and S. H. Klapp, “Irreversibility, heat and information flows induced by non-reciprocal interactions,” *New Journal of Physics*, vol. 22, no. 12, p. 123051, 2020.
- [12] Nagwa.com, “Lesson Explainer: Newton’s Third Law of Motion,” 2022. [Online]. Available: <https://www.nagwa.com/en/explainers/923174389174/>
- [13] A. Hudspeth, “Making an effort to listen: Mechanical amplification in the ear,” *Neuron*, vol. 59, 2008.
- [14] É. Roldán, *Irreversibility and dissipation in microscopic systems*. Springer, 2014.
- [15] D. Hartich, A. C. Barato, and U. Seifert, “Sensory capacity: an information theoretical measure of the performance of a sensor,” *Physical Review E*, vol. 93, no. 2, p. 022116, 2016.

- [16] T. Reichenbach and A. Hudspeth, “The physics of hearing: fluid mechanics and the active process of the inner ear,” *Reports on Progress in Physics*, vol. 77, no. 7, p. 076601, 2014.
- [17] T. Sungkaworn, M.-L. Jobin, K. Burnecki, A. Weron, M. J. Lohse, and D. Calebiro, “Single-molecule imaging reveals receptor–g protein interactions at cell surface hot spots,” *Nature*, vol. 550, no. 7677, pp. 543–547, 2017.
- [18] P. C. Bressloff, *Stochastic processes in cell biology*. Springer, 2014, vol. 41.
- [19] N. G. Van Kampen, *Stochastic processes in physics and chemistry*. Elsevier, 1992, vol. 1.
- [20] K. Sekimoto, *Stochastic energetics*. Springer, 2010, vol. 799.
- [21] K. Jacobs, *Stochastic processes for physicists: understanding noisy systems*. Cambridge University Press, 2010.
- [22] M. Doi, S. F. Edwards, and S. F. Edwards, *The theory of polymer dynamics*. oxford university press, 1988, vol. 73.
- [23] R. Kubo, “The fluctuation-dissipation theorem,” *Reports on progress in physics*, vol. 29, no. 1, p. 255, 1966.
- [24] D. Mizuno, D. Head, F. MacKintosh, and C. Schmidt, “Active and passive microrheology in equilibrium and nonequilibrium systems,” *Macromolecules*, vol. 41, no. 19, pp. 7194–7202, 2008.
- [25] M. A. Vollrath, K. Y. Kwan, and D. P. Corey, “The micromachinery of mechanotransduction in hair cells,” *Annual review of neuroscience*, vol. 30, p. 339, 2007.
- [26] S. v1.9.0 Manual, “scipy.signal.welch,” 2022. [Online]. Available: <https://docs.scipy.org/doc/scipy/reference/generated/scipy.signal.welch.html>

APPENDIX A

Numerical simulation of computing the Autocorrelation function

We implemented the numerical simulation of the autocorrelation function in the fourier space (also known as power spectral density (PSD)) using Python.

The PSD of the position of the Brownian particle is defined in Ref. [14] as:

$$PSD_x(\omega) = \frac{|\tilde{x}(\omega)|^2}{T} \quad (\text{A.1})$$

where \tilde{x} is the fourier-transform of the position of the Brownian particle, and T is the measurement of time

In our implementation in Python, we use the Welch method [26]:

```
scipy.signal.welch
```

wherein this method segments the whole data (N) into smaller segments (n). For each n , we compute for the PSD as defined in Equation(A.1), then we take the average over all n . This method outputs f = array of sample frequencies, and P_{xx} = Power spectral density of x .

Here below is the exact parameters that we used to generate the numerical simulation of the autocorrelation function as shown in Figures 3.8(b), 3.9(b), and 3.15.

```
f, power_spectrum = scipy.signal.welch(x = data, fs = 1/0.01, nperseg=1000000)
```

where x refers to the data (in our case, the trajectory of the position of hair bundle), fs refers to the sampling frequency (1/0.01ms), and $nperseg$ refers to the length of each segment.